2

NASA TECHNICAL
MEMORANDUM

NASA TM X-58046
June 1970

MONTE CARLO ANALYSIS OF STRUCTURAL LOADS RESULTING FROM SPACE VEHICLE LIFT-OFF

A Thesis Presented to the
Faculty of the University of Houston
In Partial Fulfillment of the Requirements for the Degree
Master of Science in Mechanical Engineering

NATIONAL AERONAUTICS AND SPACE ADMINISTRATION
MANNED SPACECRAFT CENTER
HOUSTON, TEXAS

NASA TM X-58046

MONTE CARLO ANALYSIS OF STRUCTURAL LOADS RESULTING FROM SPACE VEHICLE LIFT-OFF

Robert Douglas Schwartz
Manned Spacecraft Center
Houston, Texas

MONTE CARLO ANALYSIS OF STRUCTURAL LOADS RESULTING FROM SPACE VEHICLE LIFT-OFF

National Aeronautics and Space Administration
Manned Spacecraft Center
Houston, Texas

June 1970

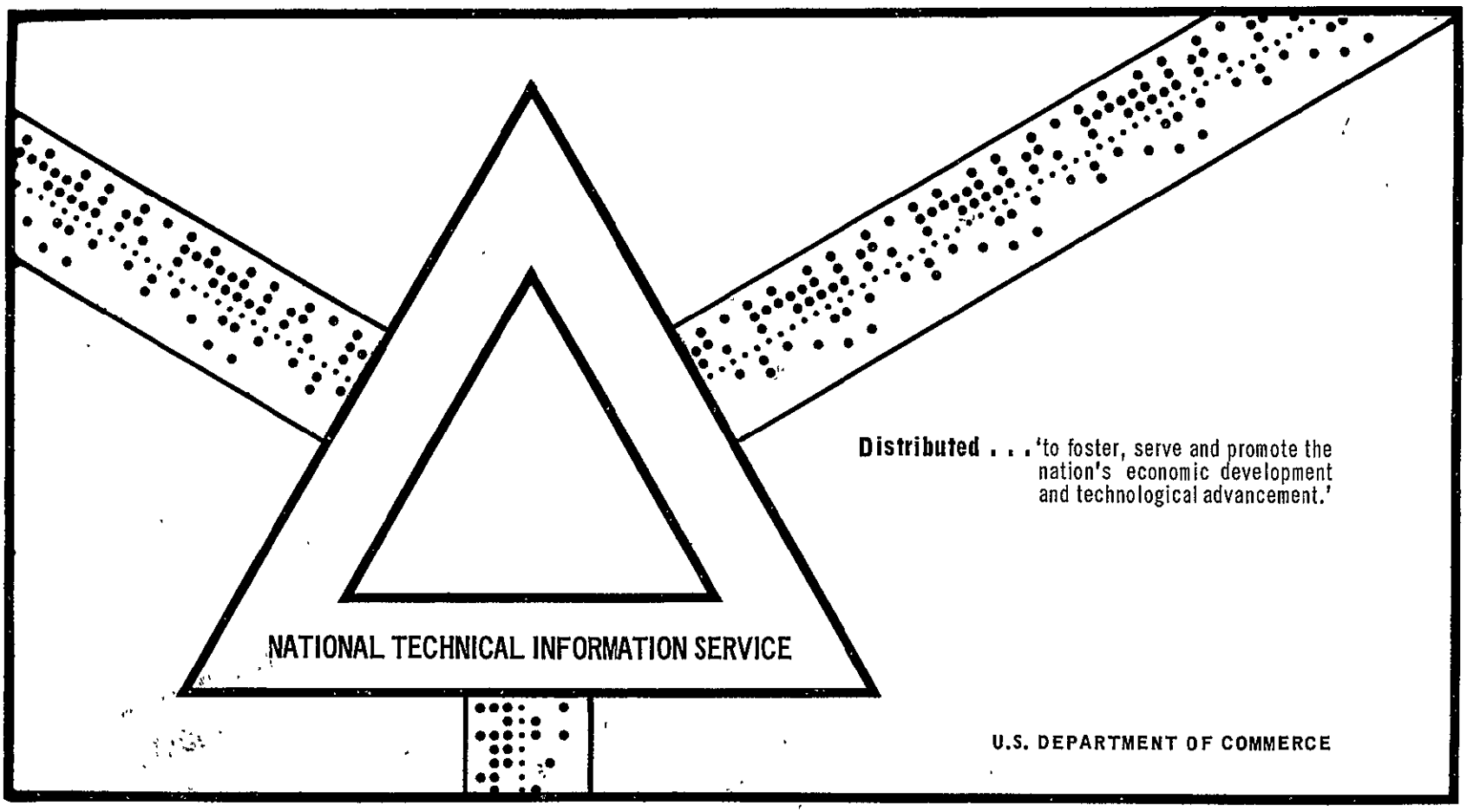

ABSTRACT

A Monte Carlo analysis was conducted to determine a theoretical Apollo Saturn V launch release design bending moment at a critical location on the spacecraft structure. Inputs to the analysis were defined by their distribution functions and selected by a random number generator. Three-dimensional structural dynamic characteristics of the Apollo Saturn V vehicle were used in a forced response program to determine the spacecraft loads for 200 cases. The results indicate that the maximum bending moment is lognormally distributed. In addition, the design bending moment was compared to one obtained using the current design method of root-sum-squaring the results of several separate cases.

This investigation shows that a Monte Carlo approach to determine a lift-off design load is feasible, and that the result obtained through the current design method is conservative.

ACKNOWLEDGEMENTS

The author wishes to express his appreciation:

To his thesis advisor, Dr. L. C. Eichberger for his invaluable technical advice;

To Dr. G. Dawkins for his kind assistance in developing the statistics theory;

To his supervisors, Messrs. George Griffith and Donald Wade for their suggestions and encouragement;

To his co-worker, Mr. Nieder for his assistance in developing computer programs; and

To his wife Barbara whose patience and understanding made this thesis possible.

TABLE OF CONTENTS

LIST OF TABLES

LIST OF ILLUSTRATIONS

NOTATIONS

$[C]$	damping matrix for structural model
$\{F_g\}$	matrix of modal generalized forces
$\{F_i(t)\}$	matrix of externally applied force time histories
F_{i_j}	force time history in j direction applied to mass i, lb
h	height above ground level, ft
h_1	reference height above ground level, ft
I_{i_j}	mass moment of inertia of m_i about axis j, lb-sec^2-in
$[K]$	stiffness matrix for structural model
$[K_g]$	matrix of modal generalized stiffnesses
M_i	bending moment at CM/SM interface about axis i, in-lb
M_R	resultant bending moment at CM/SM interface, in-lb
$M_{R_{max}}$	maximum resultant bending moment at CM/SM interface, in-lb $\times 10^{-6}$
$[M]$	mass matrix for structural model
$[M_g]$	matrix of modal generalized masses
m_i	mass at node i, lb-sec^2-in^{-1}
R_1	initial thrust buildup slope, lb/sec
R_2	final thrust buildup slope, lb/sec
S_i	shear in direction i at CM/SM interface, lb
S_R	resultant lateral shear at CM/SM interface, lb

t	simulation time, sec
V_w	windspeed at height h, knots
V_{w_R}	windspeed at reference height h_1, knots
w	coordinate system used to derive modal equations
x,y,z	coordinate directions used in math model
x_i, y_i, z_i	coordinates of mass at node i, in.
ζ	damping factor
θ_{ij}	rotation of mass i about axis j, radian
μ	mean value
$\{\xi\}$	normal coordinates
σ	standard deviation
$[\phi]$	matrix of orthogonal modes for structural model
$[\omega^2]$	matrix of the square of the modal frequencies

CHAPTER I

INTRODUCTION

Although in appearance the lift-off of a giant space vehicle is slow and majestic, structurally it can be one of the most violent and critical phases of the vehicle flight. Prior to lift-off, steady winds and gusts create thousands of pounds of lateral drag. Von Karman vortices (vortex shedding) occur at critical windspeeds and cause the vehicle to sway in a direction normal to the wind. The unsymmetric buildup of engine thrusts causes large lateral forces and torques, as well as longitudinal forces, to be applied. The application of these wind and thrust forces results in static and dynamic deflections of the vehicle and large loads in the hold-down structure. The quick release of these constraining loads induces large lateral and longitudinal structural oscillations in the structure. The design loads on a spacecraft due to these oscillations are an important design consideration and are difficult to establish because of the many variations in sequence times, thrust buildup rates, and maximum thrust. Although considerable statistical information about these parameters exists, a meaningful application to determine design loads has not yet been established. For example, the design lateral loads for the spacecraft are now determined in the following manner (Reference 1). First, a design windspeed versus altitude profile and a corresponding vortex shedding load are selected, and the bending moment

resulting from a lift-off in that wind is calculated. Next, a combination of thrust buildup forces is selected which produces maximum excitation of the cantilevered vehicle. The bending moment resulting from lift-off during this excitation is calculated. Finally, the results of the two cases are root-sum-squared to determine a design bending moment.

This design method has several drawbacks. First, design loads evolve from a selection of worst-worst inputs. Because of the complex nature of the problem it is not possible to determine whether or not this is a conservative approach. Second, the design case is hypothetical since it is not based on a realistic combination of inputs. Therefore, the probability of its occurrence is unknown. These drawbacks, plus the availability of statistical input data, have led to the evolution of the Monte Carlo approach of calculating lift-off loads.

The objective of this investigation is to develop a means of statistically analyzing spacecraft loads at lift-off through the use of the Monte Carlo method. This method is a solution of a problem in which the input data for many cases are selected at random through the use of a table of random numbers and probability distributions of the inputs. Selected outputs of the problem are then analyzed statistically by constructing their probability distributions from the results of many cases. This investigation will apply the technique to determine the Apollo Saturn V vehicle spacecraft loads at thrust buildup and launch release. Probability distributions of windspeed and direction, engine start times, buildup rates, maximum thrust levels and engine alignments, and launch release time will first be established. Using a table of random numbers, data for 200 cases will be selected from the probability distributions.

The data for each case will be used to set up force time histories and sequences of events. Using a digital computer solution, these forces will then be applied to a structural mathematical model of the Apollo Saturn V and maximum spacecraft structural loads calculated for each case. The peak loads for the 200 cases will then be ordered from lowest to highest, a mean and standard deviation established, and a probability distribution plotted. This distribution will then be used to establish a theoretical design value which will be compared both in magnitude and meaning to one obtained by the current design method of solution.

CHAPTER II

EQUATIONS OF MOTION

The method used to solve for the dynamic response of the space vehicle utilizes the standard normal mode equations with viscous damping. A basic description of the method follows, and a more rigorous derivation may be found in Reference 2.

Consider the Apollo Saturn V space vehicle to be an n degree-of-freedom lumped parameter system with mass matrix $[M]$, stiffness matrix $[K]$, damping matrix $[C]$, and the column matrix of external forces $\{F(t)\}$ all expressed in the w coordinate system. The differential equations of motion in the w coordinate system take the form

$$[M]\{\ddot{w}\} + [C]\{\dot{w}\} + [K]\{w\} = \{F\} \tag{1}$$

In the normal mode method, mode shapes and frequencies for a system defined by Equation (1) are found from the matrix equation

$$\left\{[K] - [\omega^2 M]\right\}\{w\} = \{0\} \tag{2}$$

The solution to Equation (2) in terms of mode shapes and frequencies is found by making the matrix transformation

$$\{w\} = [\phi]\{\xi\} \tag{3}$$

in which each column of $[\phi]$ is a modal column of the system and $\{\xi\}$

are normal coordinates. Differentiating Equation (3) with respect to time leads to

$$\{\dot{w}\} = [\phi]\{\dot{\xi}\} \tag{4}$$

and

$$\{\ddot{w}\} = [\phi]\{\ddot{\xi}\} \tag{5}$$

Substituting Equations (3), (4), and (5) into Equation (1) and premultiplying by the transpose of $[\phi]$, Equation (1) becomes

$$[\phi]^T[M][\phi]\{\ddot{\xi}\} + [\phi]^T[C][\phi]\{\dot{\xi}\} + [\phi]^T[K][\phi]\{\xi\} = [\phi]^T\{F\} \tag{6}$$

But the orthogonality relationship among normal modes is expressed by

$$\{\phi_i\}^T[M]\{\phi_j\} = 0 \qquad i \neq j \tag{7}$$

$$\{\phi_i\}^T[K]\{\phi_j\} = 0 \qquad i \neq j \tag{8}$$

Therefore

$$[\phi]^T[M][\phi] = [M_g] \tag{9}$$

where $[M_g]$ is the matrix of generalized masses, and

$$[\phi]^T[K][\phi] = [\omega_r^2][M_g] = [K_g] \tag{10}$$

Comparison of the triple matrix product $[\phi]^T[C][\phi]$ with Equations (9) and (10) shows that the product results in a diagonal matrix only when $[C]$ is proportional to either $[M]$ or $[K]$. Making the assumption $[C] = 2\zeta[M]$, then

$$[\phi]^T[C][\phi] = 2\zeta[M_g] \tag{11}$$

Expressing $[\phi]^T\{F\}$ by $\{F_g\}$, the generalized forces, and substituting Equations (9), (10), and (11), Equation (6) becomes

$$[M_g]\{\ddot{\xi}_r\} + 2\zeta[M_g]\{\dot{\xi}_r\} + [\omega_r^2][M_g]\{\xi_r\} = \{F_g\} \tag{12}$$

Equation (12) then is the standard form of the normal mode equations which can be used to calculate the dynamic response of the space vehicle. A description of the structural model is included in Chapter III.

CHAPTER III

STRUCTURAL MODEL

The structural model used in the analysis is a 180-degree-of-freedom lumped mass model of the Apollo Saturn V vehicle (Figure 1). Fifty lumped masses were configured to match the mass properties of the fourth Apollo Saturn V vehicle (Apollo 9). A composite total vehicle lumped mass model was constructed by North American Rockwell Corporation from mass and stiffness matrices of the spacecraft provided by NASA Manned Spacecraft Center and of the launch vehicle provided by NASA Marshall Space Flight Center.

The lumped mass models of each of the components making up the entire vehicle are shown in Figures 2 through 6. For reference purposes, the 50 lumped masses (hereafter called nodes) are numbered consecutively from the top of the spacecraft to the base of the launch vehicle. Figure 2 shows the launch escape system (LES) and command module (CM) portions of the spacecraft. The service module (SM), housing spacecraft life support systems, spacecraft propulsion system, and fuel and oxidizer tanks, is illustrated in Figure 3. Figures 4 and 5 are the lumped mass descriptions of the lunar module (LM) and its housing and the spacecraft LM adapter (SLA), respectively. The nodal description of the three-stage launch vehicle is illustrated in Figure 6. The coordinates of the entire lumped mass system are listed in Table I and are consistent with the coordinate system of Figure 1. Also shown in the table are the degrees of freedom retained for each mass point.

Orthogonal modes and frequencies for the launch vehicle were calculated by North American Rockwell Corporation using the Givens Method (Reference 3). Two sets of modes were calculated and subsequently used in the analysis. The first set is for the ignition phase, wherein the vehicle is still held down on the launch pad (cantilevered). A total of 91 cantilever modes were calculated, 30 of which are used in this study. The second set of modes calculated were for the lift-off or free-free configuration. A total of 84 free-free modes were calculated, 30 of which are used in the study. Modal damping equal to 1 percent of critical damping is used in the analysis for all cantilever and free-free modes.

CHAPTER IV

LOADS EQUATIONS

The Apollo spacecraft is a very complex structure requiring complicated stress analyses to trace load paths for a given set of body loads. As indicated in the introduction, however, the objective of this investigation is to derive a method for determining a realistic set of basic body loads for the design condition of lift-off. A description of the stress analysis stemming from the calculation of body loads is therefore not within the scope of this work.

Hereafter, the term "body loads" will refer to the combination of shears, axial forces, and bending moments existing at a particular location on the spacecraft and resulting from externally applied forces and inertia forces. Although a running distribution of body loads is necessary to structurally design the spacecraft, such a distribution usually evolves from the calculation of body loads. The critical locations are generally the interfaces where major portions of the spacecraft are mated. Examples on the Apollo spacecraft are the LES/CM, CM/SM, SM/SLA, and the LM/SLA interfaces. Although it is necessary to establish body loads at all of these interfaces, this investigation will consider only the CM/SM interface as a typical and critical example. Figure 7 illustrates the math model lumped mass representation of the spacecraft above the CM/SM interface. The body loads to be calculated are those acting upon the SM side of the interface and their signs are considered positive in the direction shown. The loads are calculated from a summation of externally

applied forces and inertia forces above the interface. Externally applied forces above this interface consist entirely of wind-induced lateral forces. The inertia forces result from rigid and elastic body accelerations discussed in the previous chapter. Note that rotational degrees of freedom were not included in the modeling of the LES and are therefore not included in inertia terms of the load equations. The body loads at CM/SM interface are claculated from the following equations.

I. AXIAL FORCE

$$S_x = -\sum_{i=1}^{3} m_i \ddot{x}_i \tag{13}$$

where the m_i's are the lumped masses and the $\ddot{x}_i$'s are their total rigid and elastic body acceleration components in the x direction. A positive force indicates a tension axial force at the interface.

II. SHEAR FORCES

$$S_y = \sum_{i=1}^{3} F_{i_y} - \sum_{i=1}^{3} m_i \ddot{y}_i \tag{14}$$

$$S_z = \sum_{i=1}^{3} F_{i_z} - \sum_{i=1}^{3} m_i \ddot{z}_i \tag{15}$$

$$S_R = \sqrt{\left(S_y^2\right) + \left(S_z^2\right)} \tag{16}$$

where F_{i_y} and F_{i_z} are the y and z components, respectively, of externally applied forces and S_R is the total shear at the CM/SM interface.

III. MOMENTS

$$M_x = -I_{3_x}\ddot{\theta}_{3_x} + m_3 z_3 \ddot{y}_3 - m_3 y_3 \ddot{z}_3 \tag{17}$$

where M_x is the torsional load about the x axis at the CM/SM interface, I_{3_x} is the mass moment of inertia of the command module, and $\ddot{\theta}_{3_x}$ is its rotational acceleration about the x axis. The second and third terms in the equation result from the slight offset of the CM center of gravity from the x axis. There are no externally applied torsional forces at lift-off.

$$M_y = -\sum_{i=1}^{3} F_{i_z}\left(x_i - x_{CM/SM}\right) - I_{3_y}\ddot{\theta}_{3_y} + \sum_{i=1}^{3} m_i \ddot{z}_i\left(x_i - x_{CM/SM}\right) - m_3 z_3 \ddot{y}_3 \tag{18}$$

$$M_z = \sum_{i=1}^{3} F_{i_y}\left(x_i - x_{CM/SM}\right) - I_{3_z}\ddot{\theta}_{3_z} - \sum_{i=1}^{3} m_i\ddot{y}_i\left(x_i - x_{CM/SM}\right) + m_3 y_3 \ddot{x}_3 \tag{19}$$

$$M_R = \sqrt{\left(M_y^2\right) + \left(M_z^2\right)} \tag{20}$$

where M_y, M_z, and M_R are the y and z components and total bending moments, respectively, at the CM/SM interface. The term $(x_i - x_{CM/SM})$ represents the x-axis distance from each lumped mass to the interface. The final terms in Equations (18) and (19) again result from the offset CM mass.

CHAPTER V

INPUT DATA

As noted in the introduction, the purpose of this thesis is to determine by means of a Monte Carlo analysis the spacecraft structural loads resulting from 200 separate lift-off cases. Each case is composed of a set of discrete force time histories applied to the structural model and the model response to the forces. This section will describe how discrete forces for each case are developed from both fixed data and those data described by probability distributions. The data may generally be classified as sequencing, environmental, or propulsion.

I. SEQUENCING DATA

An important aspect of the launch release problem is the sequence of events. Variations in ignition or launch release times can have considerable impact on the ensuing structural loads.

The nominal lift-off sequence for the Apollo Saturn V vehicle is shown in Figure 8. The sequence begins at -5.4 seconds by an accurate timing device, although nothing significant to the structural simulation occurs until 0.0 second. Because the Saturn V first stage has five engines, the ignition signals are planned nominally to have as little dynamic effect as possible on the launch release. This is accomplished by staggering the start times to minimize longitudinal excitation and torques or side forces applied by the thrust buildup. Figures 8 and 9 illustrate how this is accomplished. Engine 5, the center engine,

receives the ignition signal at 0.47 second. The remaining engines are nominally ignited in diametrically opposing pairs at 0.3-second intervals thereafter. At 3.5 seconds the chamber pressures of all five engines are sensed, and if all have attained 90 percent of nominal thrust, a launch commit signal is given to retract the hold-down arms constraining the vehicle to the pad. These arms nominally release 0.22 second after the commit signal, or at 3.72 seconds.

Although the timer is exceptionally accurate, the sequence is never exactly nominal due to time variances in actual engine ignitions and hold-down arm retraction after the signal has been transmitted. Enough data, however, have been attained through tests to describe the probability distributions of these time variations. Variation in ignition time of each engine is described by its probability distribution in Figure 10. The distribution is normal with a mean of 0.0-second time variation from the nominal sequence time and a standard deviation of 0.055 second from the mean. The probability distribution of launch release delay (time from launch commit to hold-down arm retraction) is shown in Figure 11. As indicated, the nominal launch release time is 3.72 seconds, which represents a mean of 0.22 second in launch release delay.

II. PROPULSION DATA

A means of statistically describing the thrust buildup of the Saturn V engines at first appears remote because of variation in ignition time, buildup slopes, and maximum thrust. However, a close

investigation of the buildup characteristics reveals a characteristic shape to the curve. It is this characteristic or nominal shape (Figure 12) and statistically described variations from it that permit thrust buildups to be constructed for the Monte Carlo study.

The buildup curve of Figure 12 is characterized in the following manner. The time t_2 is determined from the sequence statistics already described. The first portion of the buildup (from A to B) varies little from engine to engine. The buildup from B to C is marked by a rapid buildup rate R_1, which varies from engine to engine. Once again the buildup is marked by a characteristic plateau (C-D) before entering another rapid buildup portion (D-E) with rate R_2. The last portion of the thrust buildup (E-F) is a leveling off to the maximum thrust. The probability distributions used with ignition sequence distributions to construct the thrust buildup curves are shown in Figures 13, 14, and 15. Figures 13 and 14 show the distributions of the rates R_1 and R_2, respectively. Figure 15 gives the distribution of maximum thrust.

Another important factor in the construction of thrust magnitudes is thrust direction. All five engines are nominally directed so that their thrust at ignition will act parallel to the longitudinal axis of the vehicle. Through an accurate measurement of many engine alignments after vehicles have been stacked, enough data have been gathered to construct a statistical distribution of engine alignments. These alignments are expressed in terms of two actuator positions for each engine (Figure 9). The vectors indicate the direction of a positive engine alignment for each actuator position. Lateral components of thrust

vectors would then be directed in the opposite direction. The available data on alignments indicate that they are similar for both actuator positions. The data are represented by its probability distribution in Figure 16 which is used for both actuator positions and for each of the five engines.

III. WIND DATA

Probably the most important influence on the launch release lateral loads is that of surface winds. The lateral drag and wind-induced vortex shedding are largely responsible for the lateral loads at the base of the vehicle. It is the quick release of these constraining forces that causes the dynamic response of the vehicle at lift-off.

The wind data are based on 14 years of anemometer data collected in the Cape Kennedy area. In order to establish the wind forces on the vehicle, it is first necessary to establish wind direction, gust characteristics, and a windspeed-altitude profile. The windspeed-altitude profile is established by an empirical formulation. Because the earth surface exerts a frictional force on the lower layers of the atmosphere, the speed-altitude profile is usually determined from the "power law" equation

$$V_W = V_{W_R}\left(\frac{h}{h_1}\right)^P \tag{21}$$

where V_W is the windspeed at height h and V_{W_R} is the windspeed at a reference height h_1. The exponent P is a function of windspeed and

ground roughness. For design purposes and for this thesis a value of 0.2 is used. An example of this windspeed-altitude profile is shown in Figure 17(a).

In addition to the steady-state wind profile, a time history gust shape must be assumed. This gust shape (Figure 17(b)) is represented by a wedge with linear increase to the peak wind in 2 seconds and a linear decay to steady-state wind in 2 seconds. Substantial data indicate that a design gust factor of 1.4 for all altitudes is advisable and is used in this study. Actually, since it is difficult to determine steady winds from anemometer data, there are more statistical data for peak winds. Therefore, a peak wind at a reference height is first selected from its probability distribution. This wind is then divided by 1.4 to determine a steady-state wind at the reference height. Using this information with Figure 17(a) results in a windspeed-altitude-time profile. The probability distribution for peak winds at an altitude of 60 feet occurring during a 1-hour exposure period for an annual reference period is shown in Figure 18. Although these data provide enough information to establish a wind profile, an important effect on the loads is the actual time at which the peak wind occurs. After a discussion of the problem with the wind analysis group at Marshall Space Flight Center, a decision was made to use the nominal lift-off time as the mean peak wind time and assume the time to be distributed normally with a standard deviation of 0.5 second from the mean. The probability distribution for the time of wind peak is shown in Figure 19. The remaining characteristic needed to define the profile (wind direction) is described in terms of its

probability distribution in Figure 20. Another important effect due to the wind is that of Von Karman vortex shedding. This effect results from "shedding" of vortices at critical windspeeds. When the frequency with which the vortices are shed is close to a natural frequency of the cantilevered vehicle, dynamic motion is excited. The extent of vortex shedding on the Saturn V has been estimated from wind tunnel tests and the dynamic characteristics of the vehicle. The magnitude has been expressed in terms of bending moments at the base of the vehicle and is a function of both steady-state wind and direction. Because of the difficulty in expressing vortex shedding forces, an approximation must often be assumed. For this study, vortex shedding is represented by a force acting laterally on the vehicle at its center of pressure. Its magnitude is that required to produce the test-determined base bending moment for a given steady-state wind and direction. Although the resultant vortex shedding loads is a low-frequency sinusoid ($f = 0.3$ Hz), it is expressed conservatively as a constant force at the center of pressure normal to the wind direction at the time of lift-off. The plus or minus direction of this normal force is determined randomly by the flip of a coin. The vortex shedding force versus steady-state windspeed and direction curves are shown in Figure 21.

CHAPTER VI

METHOD OF SOLUTION

The determination of launch release structural loads is complicated not only by complex input data, but by the dynamic transition of the structure from a cantilevered to a free-free state. Although several approaches are possible for the solution to such a problem, the following was chosen. As described in Chapter III, two sets of orthogonal modes and frequencies were first calculated — one set for the vehicle cantilevered from the launch pad and the second for the same vehicle free-free. As illustrated in Figure 22, the external force time histories are first applied to the cantilevered vehicle and the dynamic response and loads are recorded until lift-off. The time histories of the constraining shear, axial force, and bending moment at the base of the launch vehicle are also calculated during this period.

The next step (Figure 22) is to apply to the free-free structure the same external forces plus the calculated base constraining forces (equal in magnitude but opposite in sign). In this way, the cantilever response is simulated by the free-free structure and constraining forces. The free-free simulation is allowed to continue until after lift-off by removing the constraining forces at the time of launch release. The constraints are removed by a linear decay to zero in 0.02 second. This approximates the actual time necessary to remove all constraining forces from the hold-down arms. The CM/SM interface loads are then calculated from the free-free response.

I. COMPUTER SOLUTION

Until now the discussion has been entirely theoretical without regard to the most practical aspect of the problem, the mechanization required to apply the theory and to obtain the desired results. This is achieved through the use of three electronic computer programs programmed for the Univac 1108 digital computer. Two of the programs were developed for general purpose studies by NASA contractors and are used without modification in this analysis. The third program was developed specifically for this study.

II. RANDOM INPUT GENERATION

The random input generator program (Reference 4) accepts as inputs the probability distributions described in Chapter V and, by use of a random number generator, produces the desired input for each case. The program is an operational general purpose program. As such, its operation and theory in selecting truly "random" numbers are accepted without detailed discussion. The program is denoted by "RIG."

III. FORCING FUNCTION GENERATOR

Developed especially for this study is the "SETUP" program. The program accepts as input the data randomly generated by "RIG." It applies the theory described in Chapter V to this data and outputs, on cards, all of the force time histories necessary to complete a forced response case. The program was checked with desk calculator computation. Detailed description of "SETUP" is given in Appendix B.

IV. FORCED RESPONSE PROGRAM

The third program employed in the analysis is that used to solve the equations of motion (Chapter II) for dynamic responses and the loads equations (Chapter IV) for CM/SM interface bending moment. The program is called "FLAP" (Flight Loads Analysis Program). This program was developed by North American Rockwell Corporation by modifying the program "DEMR" (Reference 4) to include the loads equations of Chapter IV. The program accepts as inputs either the cantilevered or free-free orthogonal modes discussed in Chapter III. The modal data input on magnetic tape was provided by North American Rockwell. The program also accepts the force time histories from "SETUP" on cards. Using these inputs, the program calculates rigid and elastic motions and accompanying time histories of body loads.

The flow chart showing the use of the aforementioned computer programs is shown in Figure 23.

CHAPTER VII

NUMERICAL PROBLEM

To illustrate best how the force time histories are set up from the input data and how the launch vehicle responds to these forces, a numerical problem has been selected and the details of its solution are presented in this chapter.

The case selected as an example results in a maximum CM/SM bending moment of 1.2×10^6 in-lb, a load which was exceeded no more than 5 percent of the time in 200 cases. Table II illustrates the random input data selected for this case by "RIG" from the probability distributions. The first five numbers are the variations from the nominal ighition times selected from Figure 10 for each of the five engines. Engines 2, 3, and 5 ignited early while engines 1 and 4 ignited late. The next five data points selected from Figure 13 are the buildup rates R_1 for engines 1 through 5, respectively (Figure 12). Note the rapid buildup rate of engine number 2. The next five numbers in the table are the buildup rates R_2 (Figure 12) for each of the five engines which were selected from Figure 14. The maximum thrust values for each of the engines constitute the next five data points in Table II. The distribution from which they were selected is shown in Figure 15. These randomly selected ignition times, slopes, and maximum thrust, together with the fixed thrust characteristics of Figure 12, result in the thrust buildup curves shown in Figure 24. The randomly selected alignment angles of each of the engines actuator positions were selected from Figure 16 and are also shown in Table II.

They are used with the thrust buildup curves and the "SETUP" program to establish propulsion force time histories to be applied to the structural model. These forces and moments are applied in "FLAP" to the translational and rotational degrees of freedom of the launch vehicle thrust structure.

The wind characteristics, the next three data points in Table II, were selected randomly from their probability distributions (Figures 18, 19, and 20). The wind at the 60-foot reference height peaks at 28.4 knots from a steady-state condition of 20.2 knots (Chapter V). The wind peaks 0.24 second after the nominal launch release time and is blowing from an easterly direction (θ = 85.5° from the north). Although the wind profile is now defined in a form shown in Figure 17, the lateral drag forces must be distributed along the structural model of the vehicle in lumped fashion. Drag loads are applied to 16 locations along the vehicle where y and z lateral degrees of freedom have been retained in the structural model. "SETUP" uses the wind direction speed and time of peak to break the drag into 32 force time histories, 16 each in the y and z directions at these nodes. A vortex shedding lateral force of 14,000 pounds was selected from Figure 21 using the peak wind and wind direction data already selected. As indicated in Chapter V, this force is normal to the drag force and is applied for convenience to the structural node closest to the vehicle center of pressure. One of two possible normal directions was selected randomly, resulting in the vortex shedding components. The only remaining data point to be randomly selected is the launch release delay. The delay

selected from the distribution (Figure 11) was 0.22 second, resulting in launch release at 3.72 seconds. Together with the modal data described in Chapter III, this completes the required inputs to the "FLAP" program. Because forces such as wind drag are not zero at the initiation of the case, an initial condition subroutine of "FLAP" is employed. This subroutine calculates the modal deflection of each mode required to balance initial forces such that there are no initial accelerations. The vehicle response at lift-off to the force time histories and release for this case is shown in Figures 25 and 26. Figure 25 illustrates the axial (x) and lateral (y and z) components of acceleration of node 3, which is that of the structure of the command module (Figure 2). Figure 26 shows the time histories of the CM/SM interface axial force and pitch and yaw components of bending moment. The response before lift-off is small and is not shown in the figures.

CHAPTER VIII

RESULTS

I. MONTE CARLO RESULTS

The peak resultant bending moments for 200 cases were first tabulated and then ordered from lowest to highest as indicated in Table III. Also shown in the table is the percentage of cases that were less than or equal to each case. Thus, for example, 75 percent of the peak bending moments were less than or equal to 0.656×10^6 in-lb. From the table a cumulative distribution function of $M_{R_{max}}$ (maximum bending moment $\times 10^{-6}$) was constructed as described in Appendix A. This function is shown in Figure 27. The distribution function is plotted on normal-probability paper which displays data with a normal distribution as a straight line. The closeness of a plot to a straight line on normal-probability paper is a measure of the closeness of the distribution of the data to a normal distribution. Figure 27 is indicative that the distribution of $M_{R_{max}}$ does not closely fit a normal distribution. The χ^2 test for goodness of fit (Appendix A) was therefore not attempted with distribution of $M_{R_{max}}$. Instead, the distribution function for $\log (M_{R_{max}})$ was calculated and is shown in Figure 28. Note that $\log (M_{R_{max}})$ straightened the tail of the cumulative distribution function of $M_{R_{max}}$. The sample mean and standard deviation for $\log (M_{R_{max}})$ were calculated and the assumed normal distribution function plotted in Figure 28. The χ^2 test described in Appendix A was applied to investigate the hypothesis that $\log (M_{R_{max}})$ is normally distributed. The results of the test

(Appendix C) indicate that the hypothesis of a normal distribution is acceptable. The maximum bending moment at the CM/SM interface therefore follows the normal-probability law after the logarithmic transformation. Such functions are said to be lognormally distributed.

Before determining the design load, an acceptable launch success criterion must first be established. Assume that the design load shall be that which would not be exceeded 99 times out of 100 launches. The 99-percent value of $\log (M_{R_{max}})$ from the normal distribution in Figure 28 is 0.4. This represents a bending moment of 1.5×10^6 in-lb. Thus, 1.5×10^6 in-lb is the point estimate for a load which should not be exceeded more than 1 percent of the time. The precision of the point estimate may be evaluated by means of a confidence limit. The theory required to justify the confidence limits for point estimates may be found in advanced statistics tests and is beyond the scope of this thesis. It is mentioned only to indicate that in practice, a design load should be determined from both the load distribution function and such a confidence limit. Since what is sought is a design load, a one-sided confidence limit would be required. The one-sided confidence limit for a given load level determines a load quantity which is almost always greater than the given load level. For example, consider the probability statement

$$\Pr\left[M_{.99} \leq M\right] = 0.95$$

This one-sided confidence statement means that the true, unknown 99-percent load is less than or equal to M with 95-percent confidence. The procedure for calculating M with an assumed knowledge of the

underlying probability distribution (in this case normal) is called parametric. The parametric 95-percent confidence limit for the 99-percent point estimate of $\log (M_{R_{max}})$ is 0.516. Taking the antilog, $M_{R_{max}} = 1.68$.

Thus, if this confidence limit were considered, we could say that our point estimate of a 99-percent load is 1.5×10^6 in-lb, and in addition we have 95-percent confidence that the real 99-percent load is less than 1.68×10^6 in-lb. The consideration of confidence limits is common in engineering design and therefore a likely choice for the design bending moment would be 1.68×10^6 in-lb. Before comparing this to a design load obtained by the current method of solution, a discussion of the accompanying CM/SM interface shear and axial loads is necessary, for although this interface is bending moment critical, it is impossible to design a structural interface without a complete description of loads. The results of the 200 individual simulations indicate that the range of axial loads for all cases were all similar and varied from 22,000 to 30,000 pounds compression at the time of maximum moment. Therefore, the structure should be designed for a bending moment of 1.68×10^6 in-lb and this range of axial force. While the interface structure is sensitive to ranges in bending moment and axial load, it is less sensitive to variations in lateral shear load. Nevertheless, design shear load must accompany the combination of bending moment and axial load. The CM/SM shear load ranged from 0 to 10,000 pounds in the 200 cases. Because of the large vehicle bending characteristics, bending moments were often accompanied by little or no shear. Therefore, the designer must consider the entire range of shears together with the range of axial loads and the design bending moment.

Although this thesis considers only the CM/SM interface design load, a similar procedure would be followed for all other critical interfaces.

II. CURRENT DESIGN METHOD RESULTS

In order to compare the Monte Carlo results with those obtained by the current method of solution, a "design" case was run using the same structural model and the current method. A brief description of the method follows.

The design bending moment is obtained by root-sum-squaring the time histories of loads from three separate cases. The first case calculates launch release loads resulting from application of a design wind profile. The second case is the launch release response of the vehicle to a design unsymmetrical thrust buildup. The third case is the response to design engine alignment forces. The third case is a second order effect compared to the first two and was combined with case two for this thesis.

The current design criteria specify that the vehicle must be designed to launch in 95-percent winds. These wind loads are for conservatism to be accompanied by the maximum vortex shedding load. This resulted in a peak wind of 25.2 knots and a vortex shedding load of 57,700 pounds. For case two, the criteria specify the maximum unsymmetric thrust buildup to be constructed in such a way that a maximum thrust induced torque be applied to the base of the vehicle by a combination of the ±99.73-percent engine start times, buildup slopes, and maximum thrust values for the five engines. The design alignment is specified by using

the 3σ values of the normally distributed thrust alignment. The following equation is used to define the alignment for each of the five engines.

$$\text{Design engine deflection} = \frac{1}{\sqrt{n}} \beta_{3\sigma}$$

where n indicates the number of engines (5) and $\beta_{3\sigma}$ is the 3σ alignment defined in the input data. Both cases were run using the same structural model and programs used for the Monte Carlo cases. The maximum moment resulting from the root-sum-square of the two cases was 2.97×10^6 in-lb. The current method specifies the accompanying design shear load be a range from 0 to maximum shear resulting from the design case, or 0 to 11,000 pounds. The current method also specifies that the range of axial load be defined by the peak-to-peak axial forces at the time of maximum moment. This resulted in a range of 22,000 to 30,000 pounds compression.

III. MONTE CARLO AND CURRENT CRITERIA RESULTS COMPARISON

Although the current design criteria consider a 95-percent windspeed profile, the inclusion of maximum vortex shedding load regardless of windspeed or direction and maximum applied torques due to unsymmetric thrust buildup results in a design bending moment with a very low probability of exceedence. For example, the value of 2.97×10^6 in-lb obtained by the current design method was not once exceeded in the 200 Monte Carlo cases. Comparing log (2.97), or 1.09, with the normal distribution in Figure 28 shows, in fact, that we would not expect this load to be

exceeded at least 99.99 percent of the time. This is not surprising, particularly in view of the unlikely (if not impossible) combination of wind and vortex shedding load; the latter is considered currently to be maximum regardless of windspeed or direction.

Although the bending moment varied considerably, the ranges of axial load and shear to be considered were similar for both the current and Monte Carlo methods.

IV. CONCLUSIONS AND RECOMMENDATIONS

The foregoing discussion results in the following conclusions.

a. A Monte Carlo method to determine a lift-off design bending moment at the CM/SM interface is feasible and results in a lognormal distribution.

b. The current design method apparently results in a conservative design bending moment.

c. The Monte Carlo Method can erase some of this conservatism from the designs and still produce a realistic design load with confidence.

In view of the above conclusions and the fact that this thesis constitutes a feasibility study only, the following recommendations are made.

a. The Monte Carlo Method should be pursued further as a logical approach to the determination of lift-off design loads.

b. The theory and application of confidence limits for point estimates should be investigated thoroughly in such an analysis.

c. Attempts should be made to determine correlation between input parameters and the resulting loads. For example, greater launch day operational capability could be provided if it were discovered that high loads result only from a combination of specific windspeed and direction.

REFERENCES

REFERENCES

1. External Loads and Criteria Apollo Block II Spacecraft. Space Division, North American Rockwell, SD67-1104, June 1968.

2. Hurty, Walter C., and Rubinstein, Moshe F.: Dynamics of Structure. Prentice Hall, 1964.

3. Wilkinson, J. H.: The Algebraic Eigen-value Problem. Oxford, England, Clarendon Press, 1965.

4. Apollo Lunar Landing Analysis Computer Program Users Manual Final Report. Space Division, The Boeing Company, D2-84125-13, May 1967.

5. Parzen, Emanuel: Modern Probability Theory and its Applications. John Wiley and Sons, Inc., 1960.

6. Volk, William: Applied Statistics for Engineers. New York, McGraw Hill, 1958.

TABLE I.- LUMPED MASS MODEL COORDINATES AND DEGREES OF FREEDOM

Node	Coordinates, in.			Degrees of freedom retained					
	X	Y	Z	X	Y	Z	θ_x	θ_y	θ_z
1	4209.5	0.0	0.0	1	2	3	--	--	--
2	4052.5	.0	.0	4	5	6	--	--	--
3	3798.5	-.56	6.64	7	8	9	10	11	12
4	3749.5	.0	.0	13	14	15	16	17	18
5	3586.8	.035	.221	19	20	21	--	22	23
6	3614.0	48.31	6.58	24	25	26	--	--	--
7	3665.0	48.31	6.58	--	27	28	--	--	--
8	3716.8	48.31	6.58	--	29	30	--	--	--
9	3614.0	14.83	47.75	31	32	33	--	--	--
10	3665.0	14.83	47.75	--	34	35	--	--	--
11	3716.8	14.83	47.75	--	36	37	--	--	--
12	3614.0	-48.31	-6.58	38	39	40	--	--	--
13	3665.4	-48.31	-6.58	--	41	42	--	--	--
14	3716.8	-48.31	-6.58	--	43	44	--	--	--
15	3614.0	-14.83	-47.75	45	46	47	--	--	--
16	3665.4	-14.83	-47.75	--	48	49	--	--	--
17	3691.1	-14.83	-47.75	--	50	51	--	--	--
18	3596.0	.0	.0	52	53	54	55	56	57
19	3397.6	.0	.0	58	59	60	--	--	--
20	3307.6	.0	54.0	61	62	63	--	64	65
21	3316.3	.0	-54.0	66	67	68	--	69	70
22	3316.3	-54.0	.0	71	72	73	--	74	75
23	3316.4	.0	.0	76	77	78	--	--	--
24	3316.3	54.0	.0	79	80	81	--	82	83
25	3341.2	.0	.0	84	85	86	87	88	89
26	3258.5	.0	.0	90	91	92	93	94	95
27	3101.0	.0	.0	96	97	98	99	--	--
28	2832.0	.0	.0	100	101	102	103	--	--

TABLE I.- LUMPED MASS MODEL COORDINATES AND DEGREES OF FREEDOM - Concluded

Node	Coordinates, in			Degrees of freedom retained					
	X	Y	Z	X	Y	Z	θ_x	θ_y	θ_z
29	2832.0	0.0	0.0	104	--	--	--	--	--
30	2832.0	.0	.0	105	--	--	--	--	--
31	2646.0	.0	.0	106	107	108	--	--	--
32	2747.0	.0	.0	109	110	111	112	113	114
33	2519.0	.0	.0	115	116	117	118	--	--
34	2387.0	.0	.0	119	120	121	122	--	--
35	2117.0	.0	.0	123	124	125	126	--	--
36	1848.0	.0	.0	127	128	129	130	--	--
37	1848.0	.0	.0	131	--	--	--	--	--
38	1848.0	.0	.0	132	--	--	--	--	--
39	1760.0	.0	.0	133	134	135	136	--	--
40	1664.0	.0	.0	137	138	139	140	141	142
41	1564.0	.0	.0	143	144	145	146	147	148
42	1401.0	.0	.0	149	150	151	152	--	--
43	1156.0	.0	.0	153	154	155	156	--	--
44	912.0	.0	.0	157	158	159	160	--	--
45	912.0	.0	.0	161	--	--	--	--	--
46	757.0	.0	.0	162	163	164	165	--	--
47	602.0	.0	.0	166	177	178	179	--	--
48	365.0	.0	.0	170	171	172	173	--	--
49	365.0	.0	.0	174	--	--	--	--	--
50	100.0	.0	.0	175	176	177	178	179	180

TABLE II.- EXAMPLE RANDOM INPUT DATA

Variation in engine 1 ignition time	0.00174 sec
Variation in engine 2 ignition time	-.0185 sec
Variation in engine 3 ignition time	-.0191 sec
Variation in engine 4 ignition time	.040 sec
Variation in engine 5 ignition time	-.0476 sec
Engine 1 buildup rate, R_1	4.00×10^6 lb/sec
Engine 2 buildup rate, R_1	11.76×10^6 lb/sec
Engine 3 buildup rate, R_1	4.99×10^6 lb/sec
Engine 4 buildup rate, R_1	7.64×10^6 lb/sec
Engine 5 buildup rate, R_1	5.58×10^6 lb/sec
Engine 1 buildup rate, R_2	1.69×10^6 lb/sec
Engine 2 buildup rate, R_2	1.73×10^6 lb/sec
Engine 3 buildup rate, R_2	1.49×10^6 lb/sec
Engine 4 buildup rate, R_2	1.81×10^6 lb/sec
Engine 5 buildup rate, R_2	1.32×10^6 lb/sec
Engine 1 maximum thrust	1.50×10^6 lb
Engine 2 maximum thrust	1.51×10^6 lb
Engine 3 maximum thrust	1.52×10^6 lb
Engine 4 maximum thrust	1.52×10^6 lb
Engine 5 maximum thrust	1.50×10^6 lb
Engine 1 actuator 1 misalignment	0.00835 radian
Engine 1 actuator 2 misalignment	0.00820 radian
Engine 2 actuator 1 misalignment	0.00139 radian
Engine 2 actuator 2 misalignment	0.00468 radian
Engine 3 actuator 1 misalignment	0.00518 radian
Engine 3 actuator 2 misalignment	0.00736 radian
Engine 4 actuator 1 misalignment	0.00467 radian
Engine 4 actuator 2 misalignment	0.00451 radian
Engine 5 actuator 1 misalignment	0.00685 radian
Engine 5 actuator 2 misalignment	0.0029 radian
Peak windspeed	28.39 knots
Wind direction	85.5 degrees from N
Wind peak time	3.96 sec

TABLE III.- ORDERED LOADS

Cumulative probability, percent	CM/SM interface bending moment, in-lb × 10^{-6}	Cumulative probability, percent	CM/SM interface bending moment, in-lb × 10^{-6}
0.5	0.181	17.5	0.349
1.0	.189	18.0	.349
1.5	.196	18.5	.352
2.0	.209	19.0	.353
2.5	.214	19.5	.359
3.0	.215	20.0	.362
3.5	.231	20.5	.364
4.0	.232	21.0	.368
4.5	.233	21.5	.373
5.0	.234	22.0	.379
5.5	.248	22.5	.380
6.0	.264	23.0	.386
6.5	.269	23.5	.387
7.0	.273	24.0	.389
7.5	.273	24.5	.389
8.0	.284	25.0	.390
8.5	.290	25.5	.390
9.0	.294	26.0	.390
9.5	.308	26.5	.393
10.0	.310	27.0	.394
10.5	.312	27.5	.395
11.0	.313	28.0	.398
11.5	.315	28.5	.400
12.0	.320	29.0	.400
12.5	.320	29.5	.408
13.0	.321	30.0	.412
13.5	.325	30.5	.412
14.0	.328	31.0	.412
14.5	.329	31.5	.413
15.0	.337	32.0	.415
15.5	.339	32.5	.416
16.0	.341	33.0	.419
16.5	.342	33.5	.420
17.0	.346	34.0	.421

TABLE III.- ORDERED LOADS - Continued

Cumulative probability, percent	CM/SM interface bending moment, in-lb × 10^{-6}	Cumulative probability, percent	CM/SM interface bending moment, in-lb × 10^{-6}
34.5	0.422	52.0	0.515
35.0	.428	52.5	.519
35.5	.432	53.0	.519
36.0	.435	53.5	.521
36.5	.436	54.0	.522
37.0	.436	54.5	.522
37.5	.437	55.0	.523
38.0	.437	55.5	.527
38.5	.441	56.0	.534
39.0	.446	56.5	.534
39.5	.447	57.0	.540
40.0	.447	57.5	.540
40.5	.448	58.0	.545
41.0	.451	58.5	.548
41.5	.451	59.0	.550
42.0	.456	59.5	.551
42.5	.456	60.0	.551
43.0	.457	60.5	.556
43.5	.460	61.0	.558
44.0	.461	61.5	.560
44.5	.465	62.0	.562
45.0	.470	62.5	.563
45.5	.472	63.0	.564
46.0	.473	63.5	.565
46.5	.478	64.0	.570
47.0	.479	64.5	.570
47.5	.494	65.0	.571
48.0	.495	65.5	.572
48.5	.496	66.0	.583
49.0	.501	66.5	.585
49.5	.502	67.0	.587
50.0	.505	67.5	.587
50.5	.508	68.0	.588
51.0	.512	68.5	.589
51.5	.514	69.0	.590

TABLE III.- ORDERED LOADS - Concluded

Cumulative probability, percent	CM/SM interface bending moment, in-lb × 10^{-6}	Cumulative probability, percent	CM/SM interface bending moment, in-lb × 10^{-6}
69.5	0.594	85.0	0.727
70.0	.603	85.5	.741
70.5	.608	86.0	.766
71.0	.611	86.5	.771
71.5	.612	87.0	.787
72.0	.614	87.5	.789
72.5	.614	88.0	.799
73.0	.630	88.5	.801
73.5	.637	89.0	.805
74.0	.639	89.5	.829
74.5	.654	90.0	.839
75.0	.656	90.5	.848
75.5	.664	91.0	.858
76.0	.671	91.5	.891
76.5	.671	92.0	.894
77.0	.682	92.5	.922
77.5	.686	93.0	1.022
78.0	.686	93.5	1.023
78.5	.686	94.0	1.053
79.0	.687	94.5	1.117
79.5	.697	95.0	1.202
80.0	.698	95.5	1.213
80.5	.699	96.0	1.274
81.0	.700	96.5	1.283
81.5	.706	97.0	1.408
82.0	.709	97.5	1.535
82.5	.714	98.0	1.554
83.0	.718	98.5	2.305
83.5	.721	99.0	2.455
84.0	.726	99.5	2.536
84.5	.727	100.0	2.860

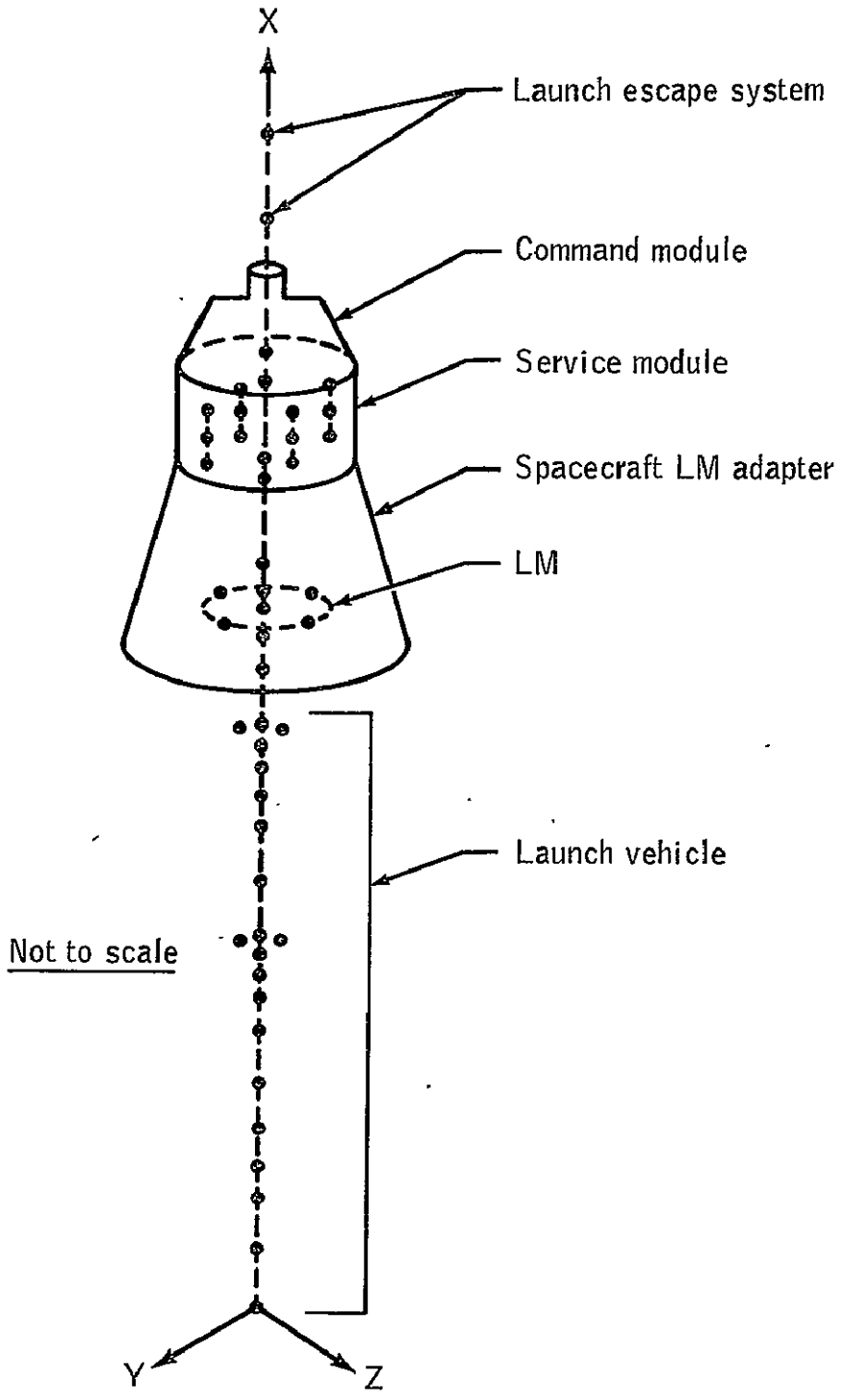

Figure 1.- Apollo Saturn V lumped mass model.

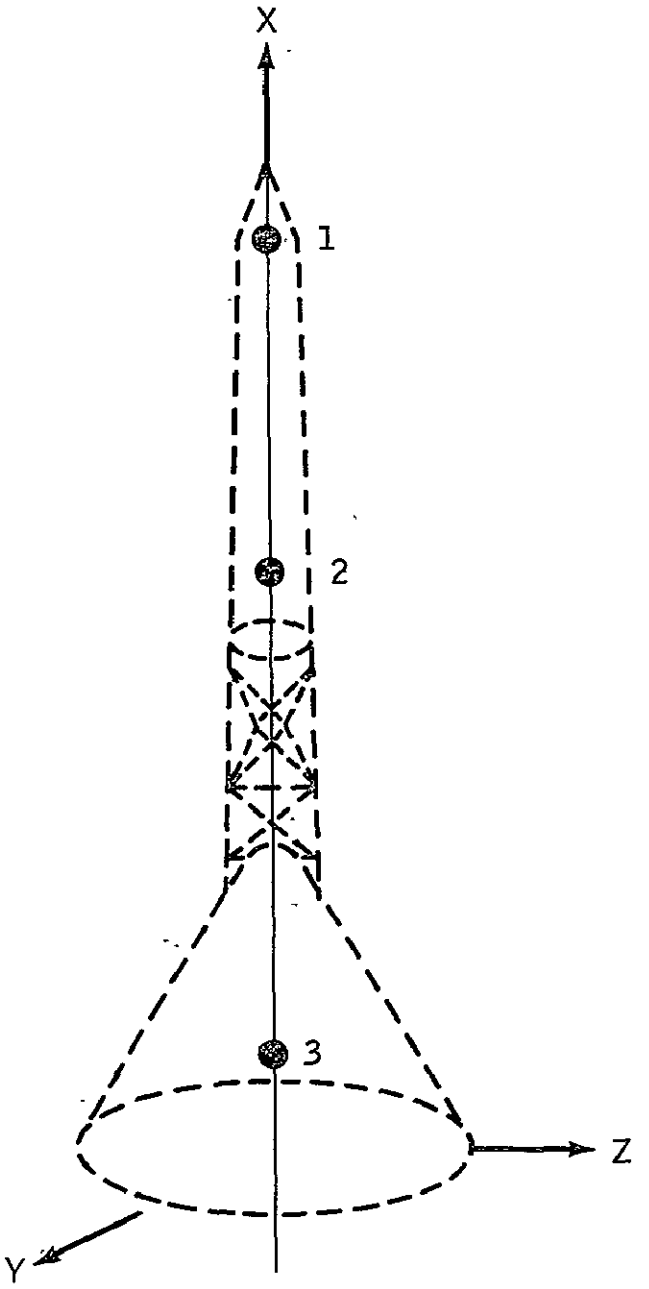

Figure 2.- Launch escape system and command module lumped mass model.

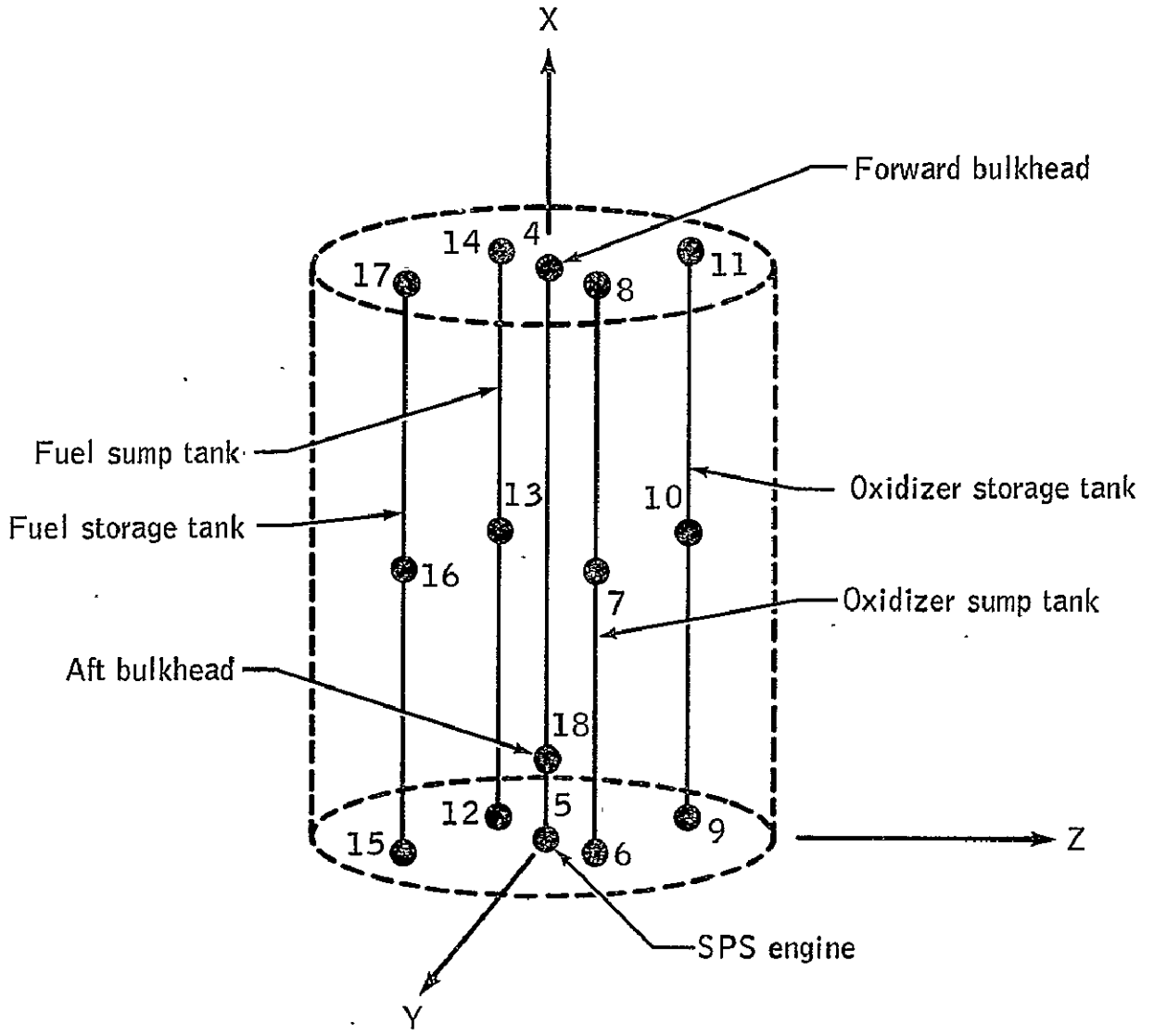

Figure 3.- Service module lumped mass model.

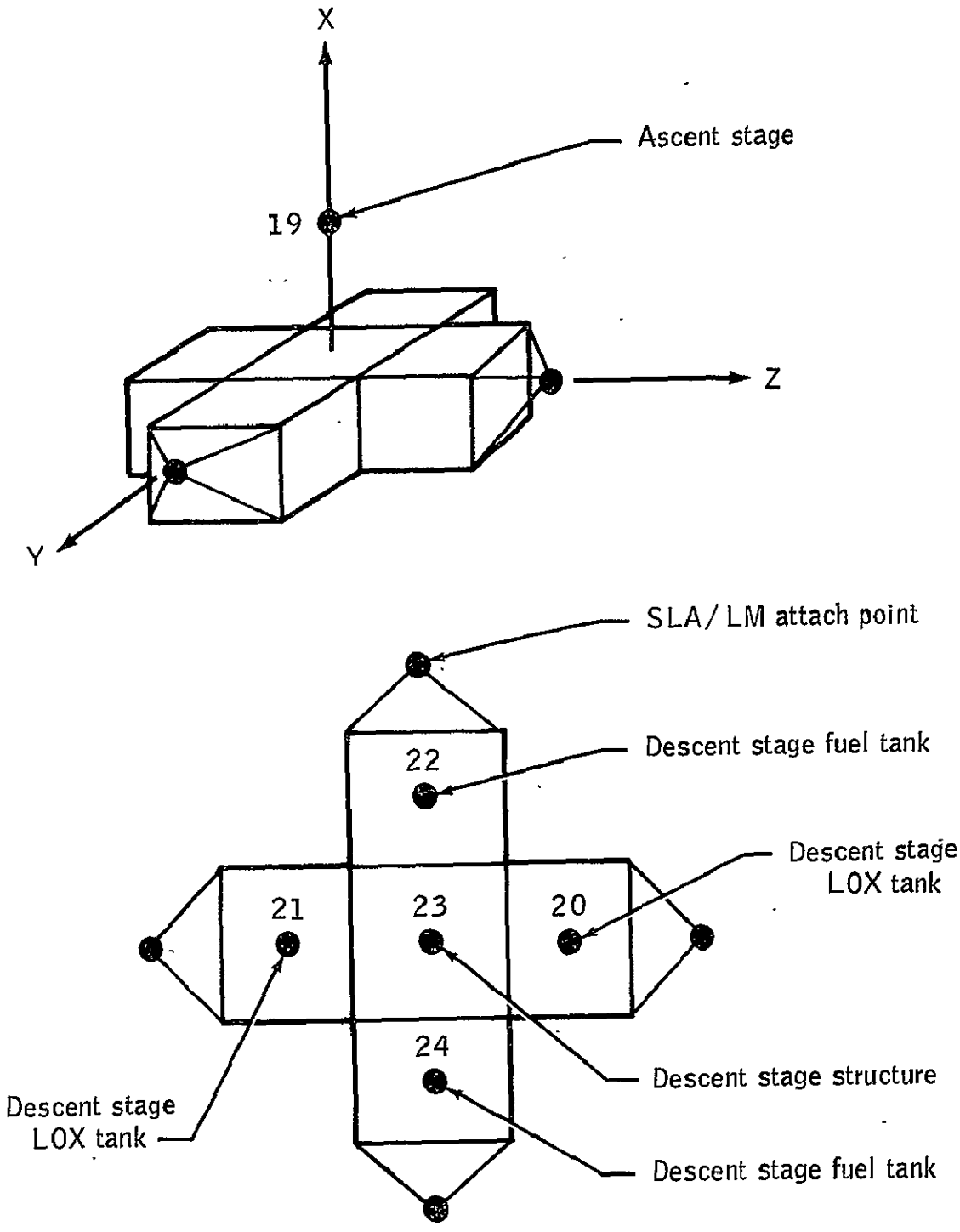

Figure 4.- Lunar module lumped mass model.

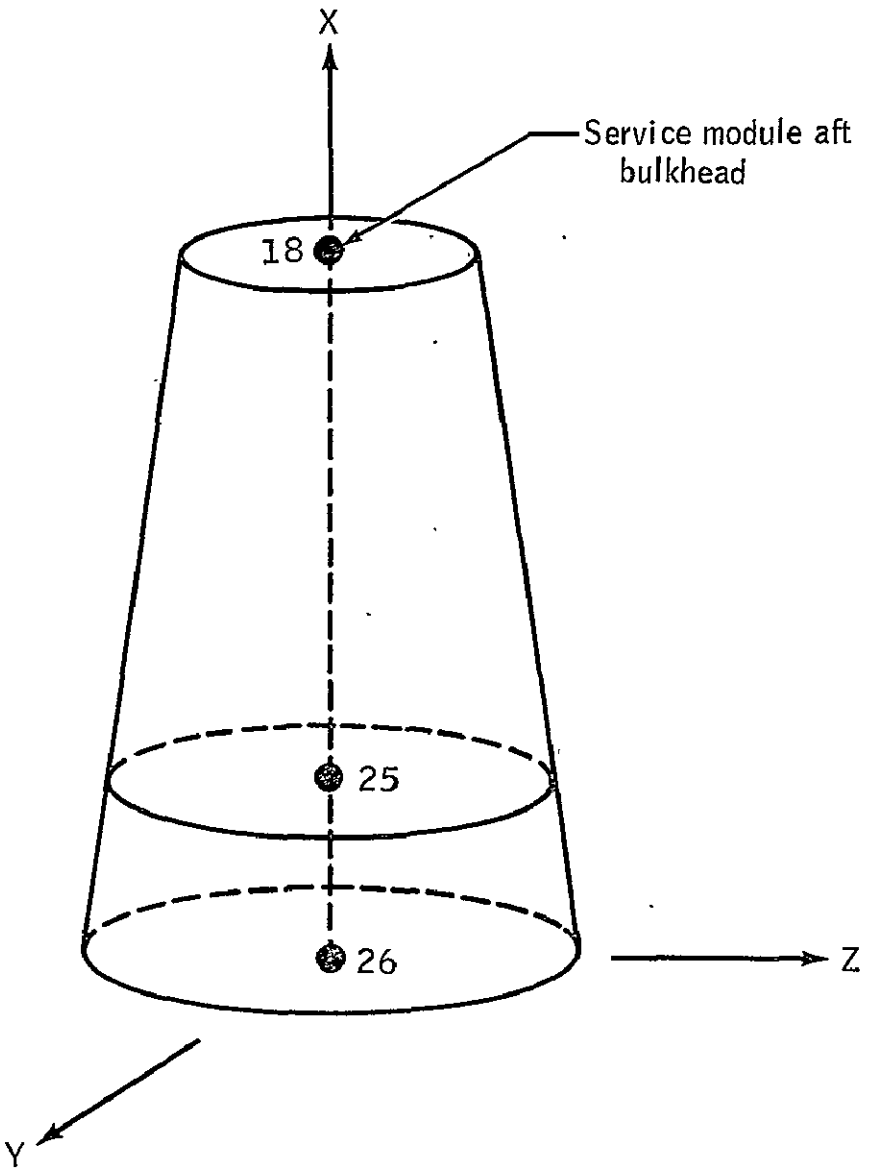

Figure 5.- Spacecraft/lunar module adapter lumped mass model.

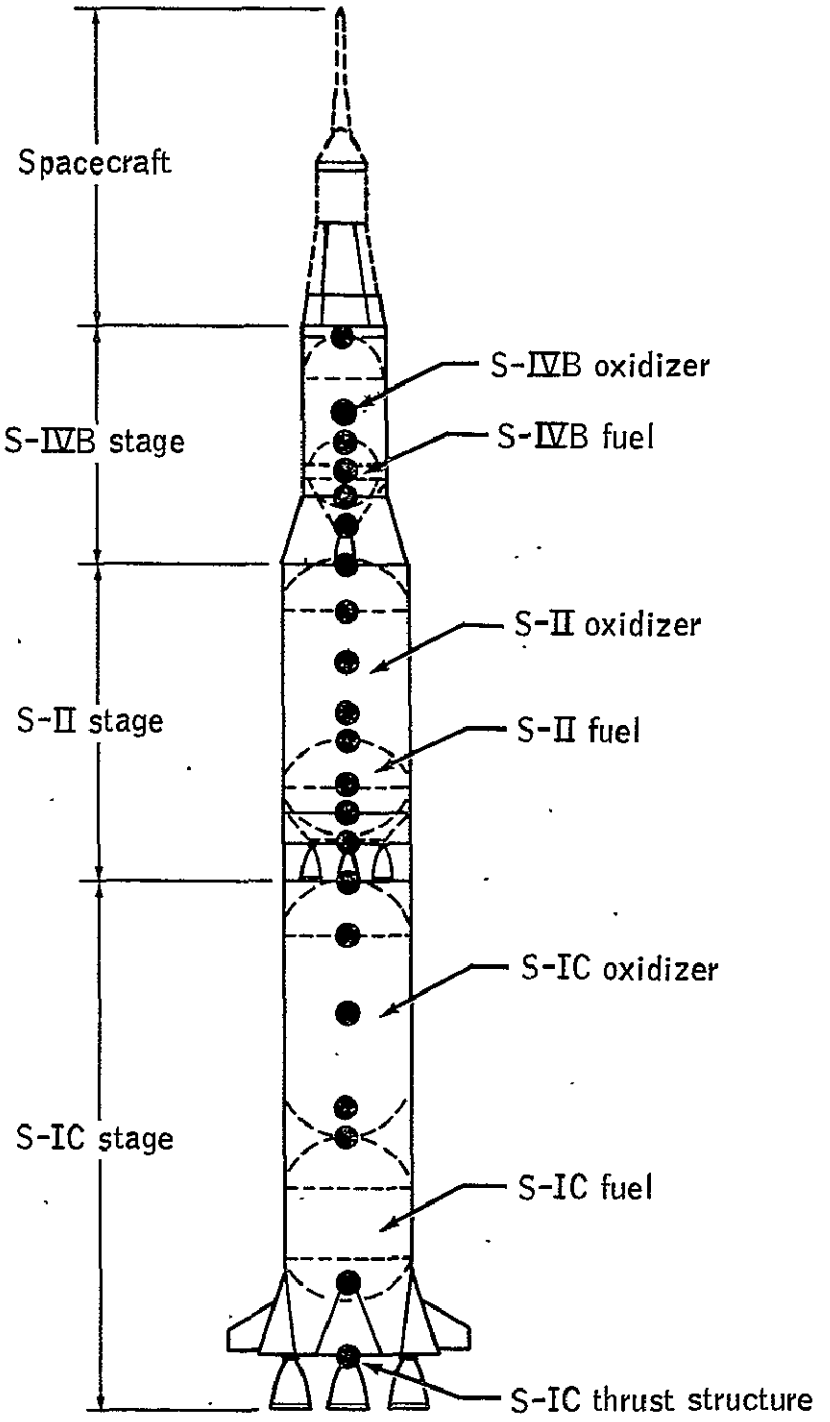

Figure 6.- Launch vehicle lumped mass model.

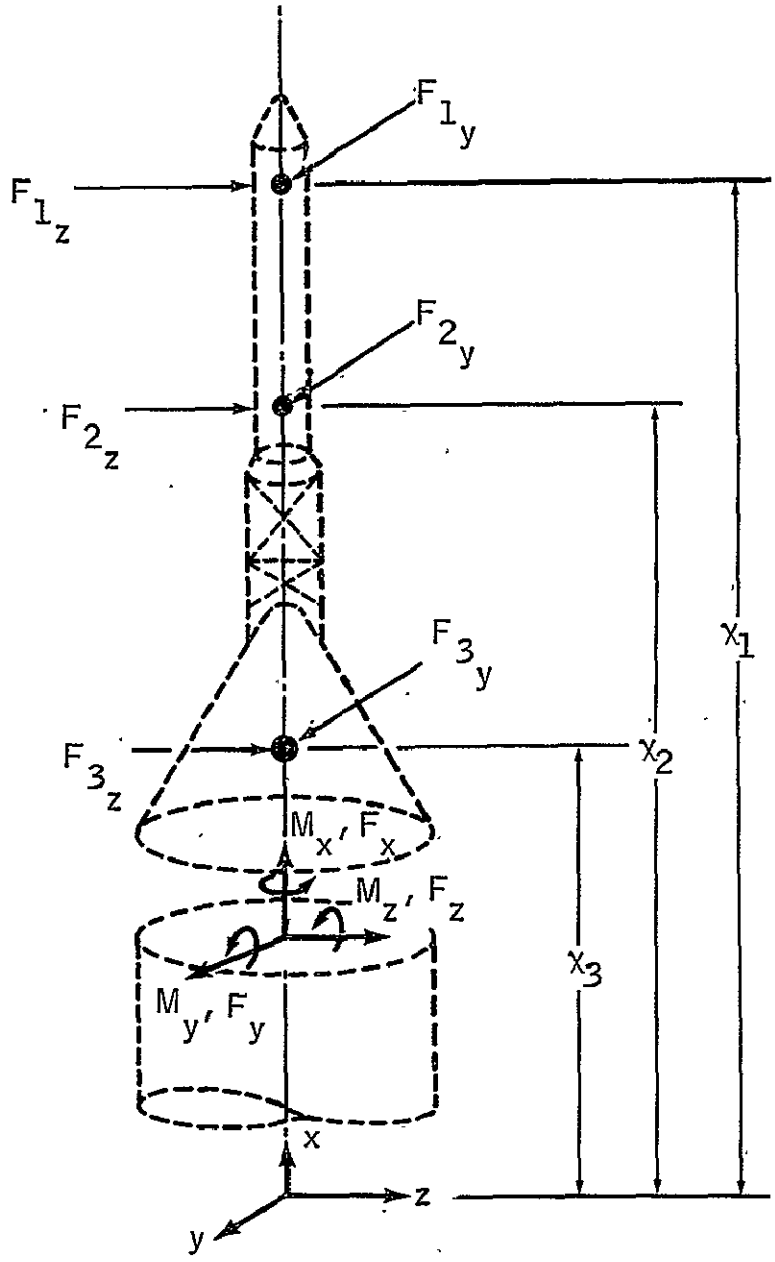

Figure 7.- Sign convention of forces acting on spacecraft and resultant loads.

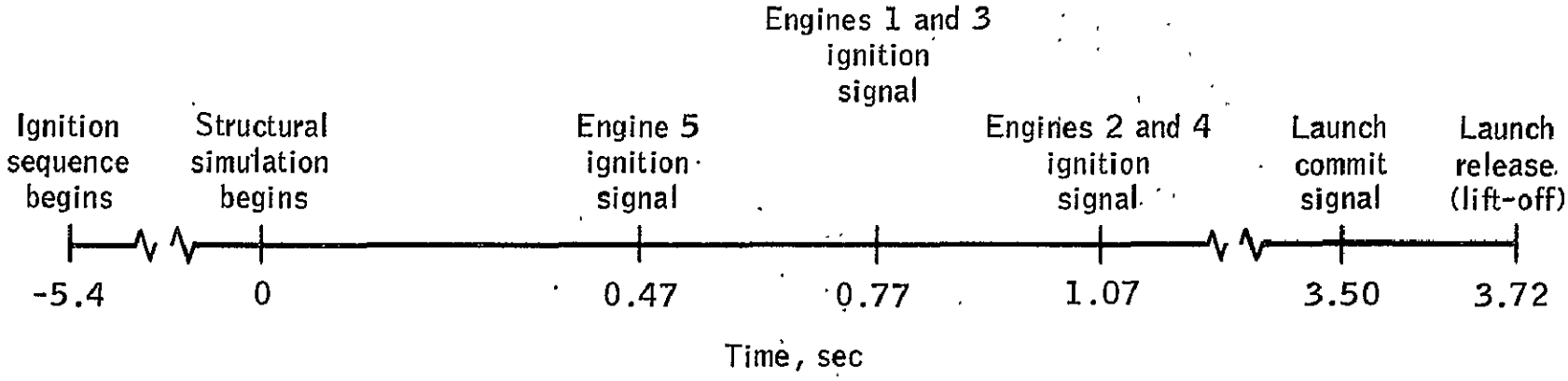

Figure 8.- Nominal Saturn V lift-off sequence.

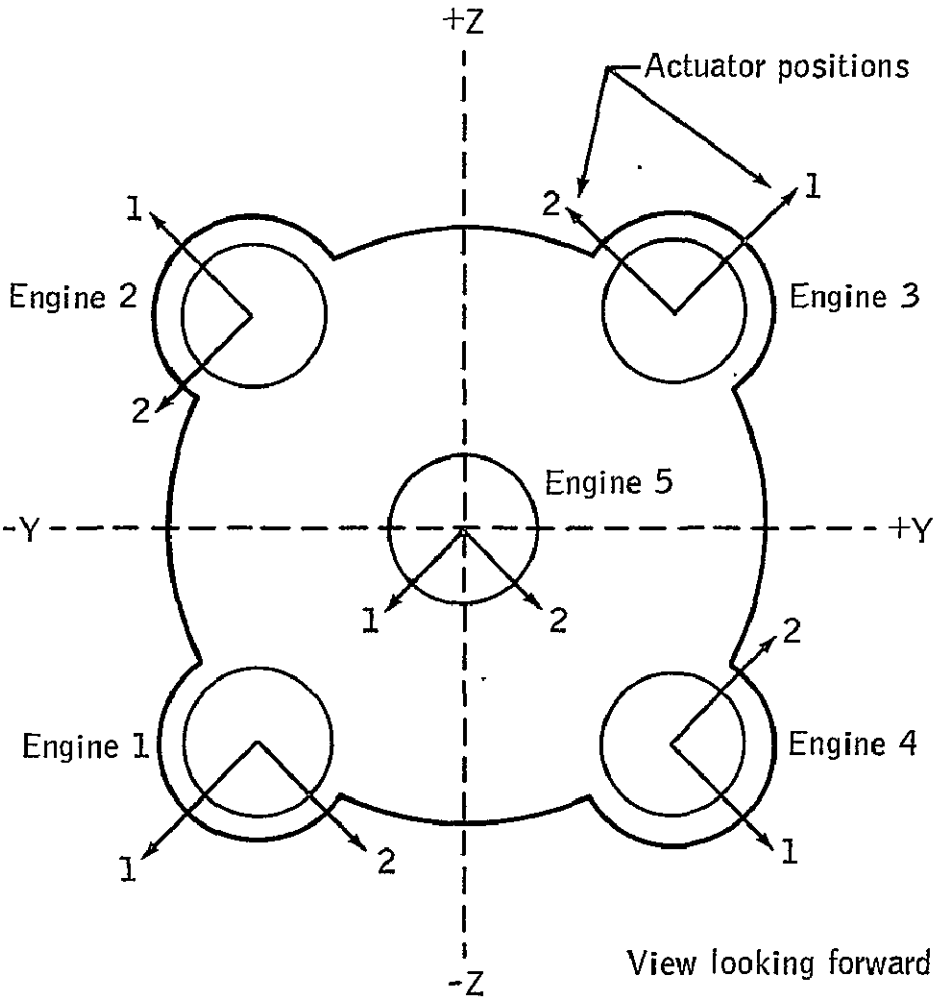

Figure 9.- Placement of Saturn V engines.

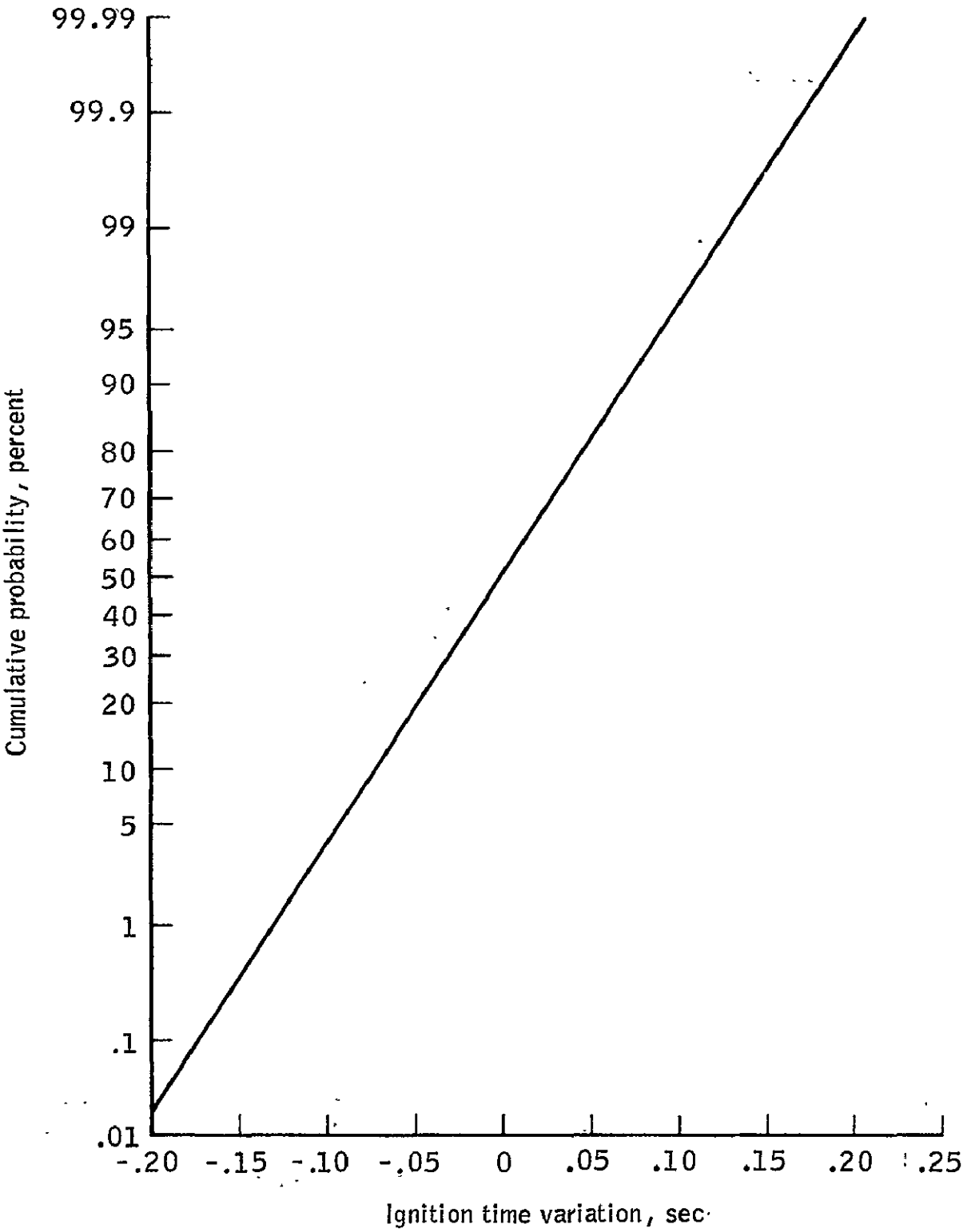

Figure 10.- Cumulative probability distribution of variation in engine ignition time.

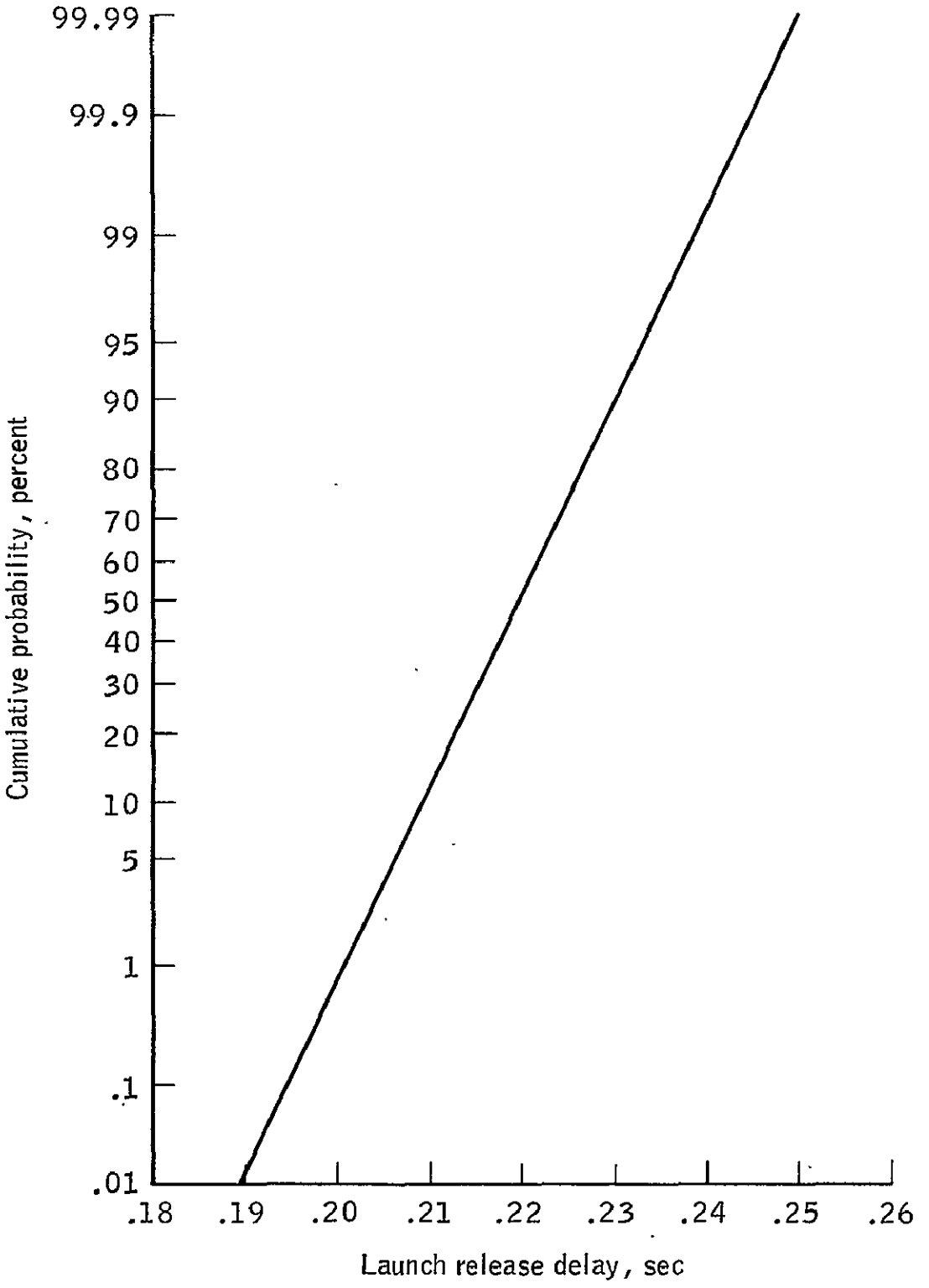

Figure 11.- Cumulative probability distribution of launch release delay.

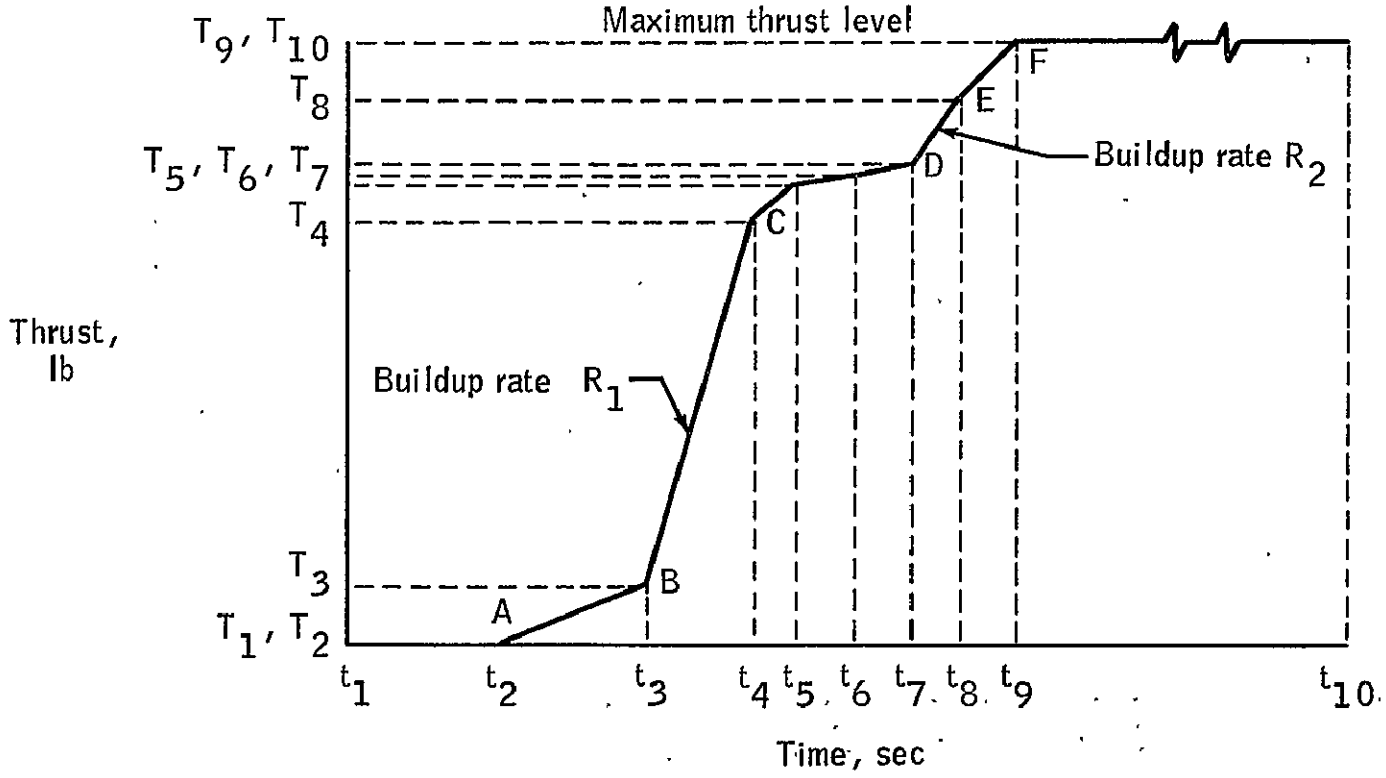

Figure 12.- Thrust buildup curve.

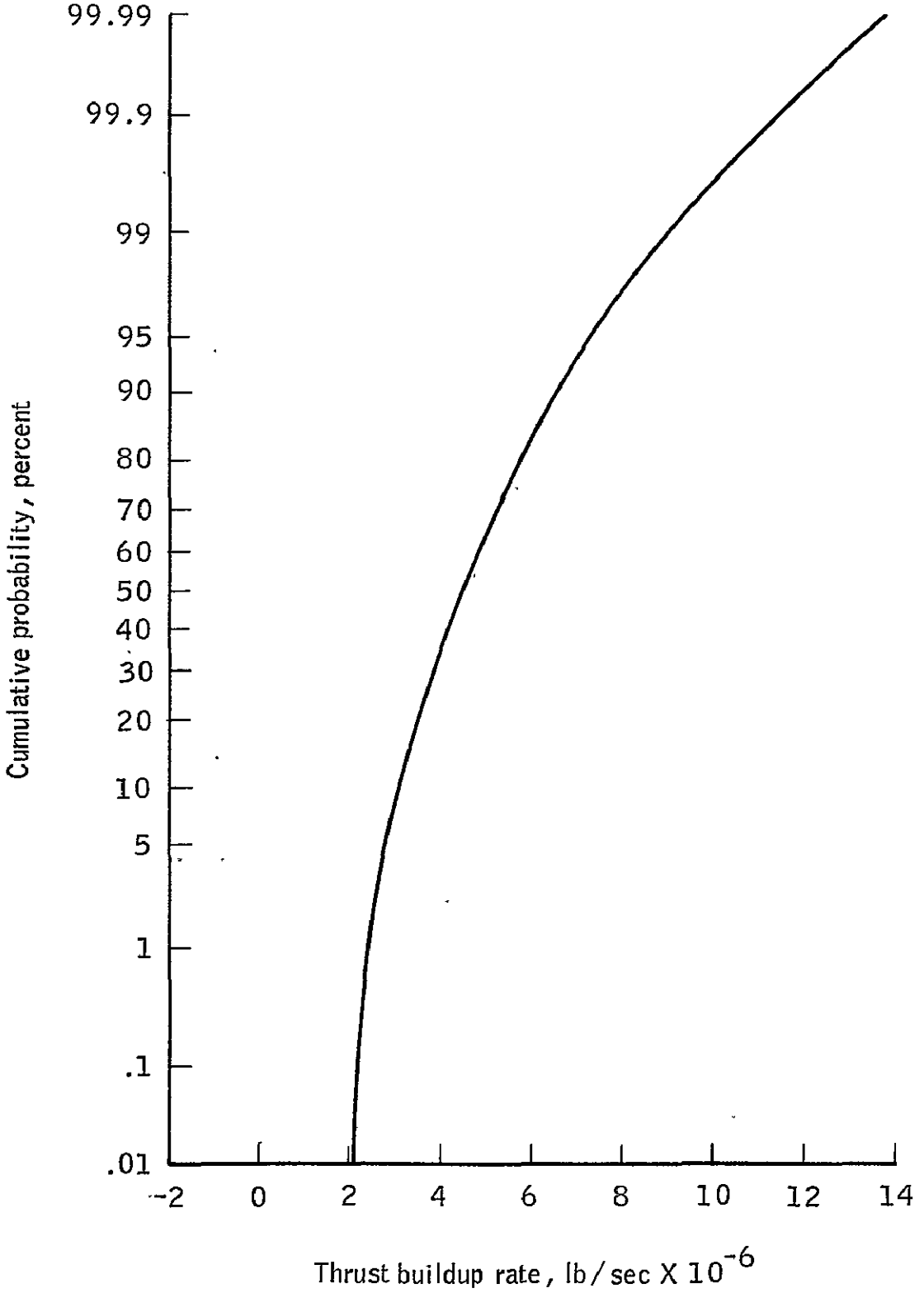

Figure 13.- Cumulative probability distribution of thrust buildup rate R_1.

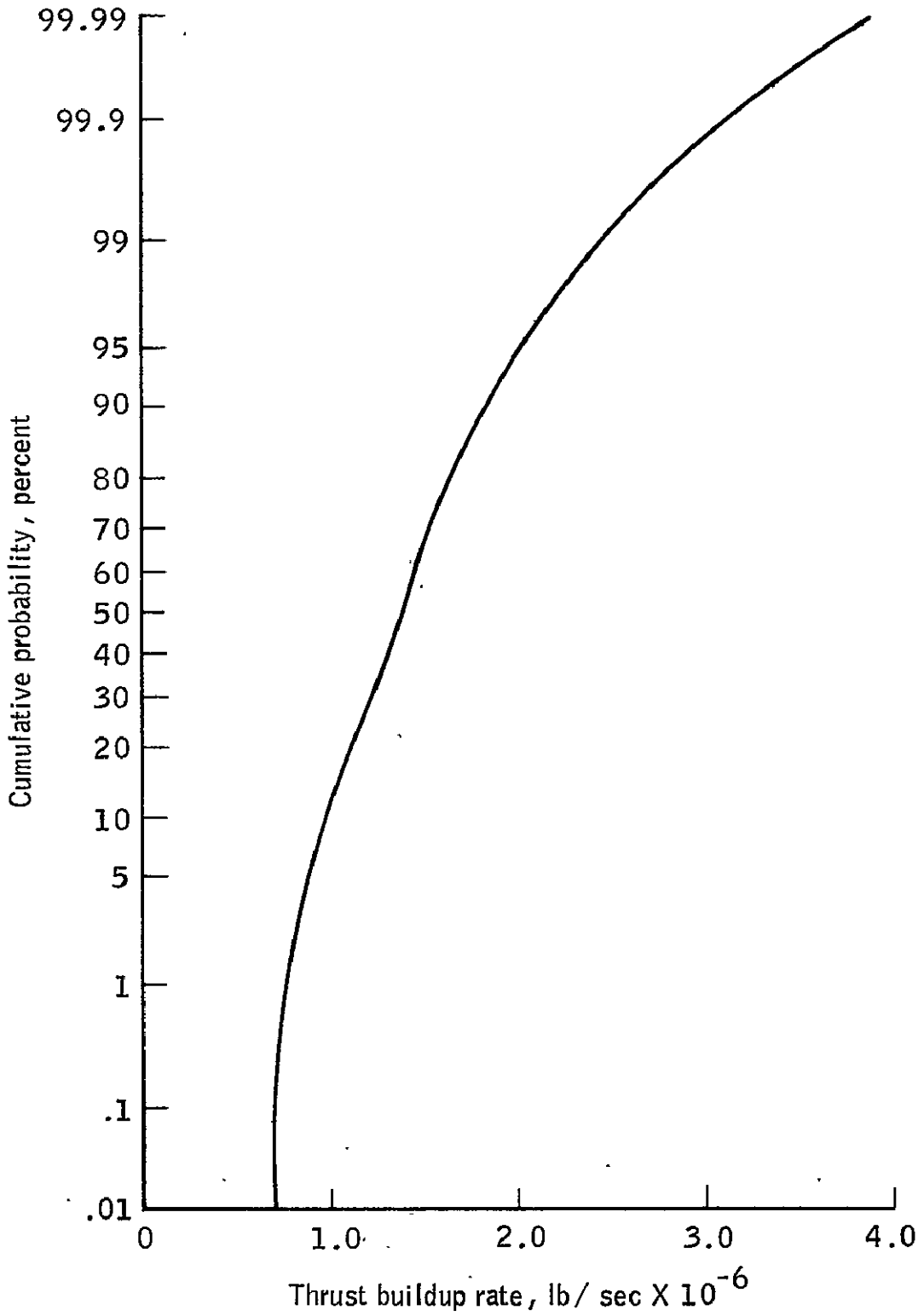

Figure 14.- Cumulative probability distribution of thrust buildup rate R_2.

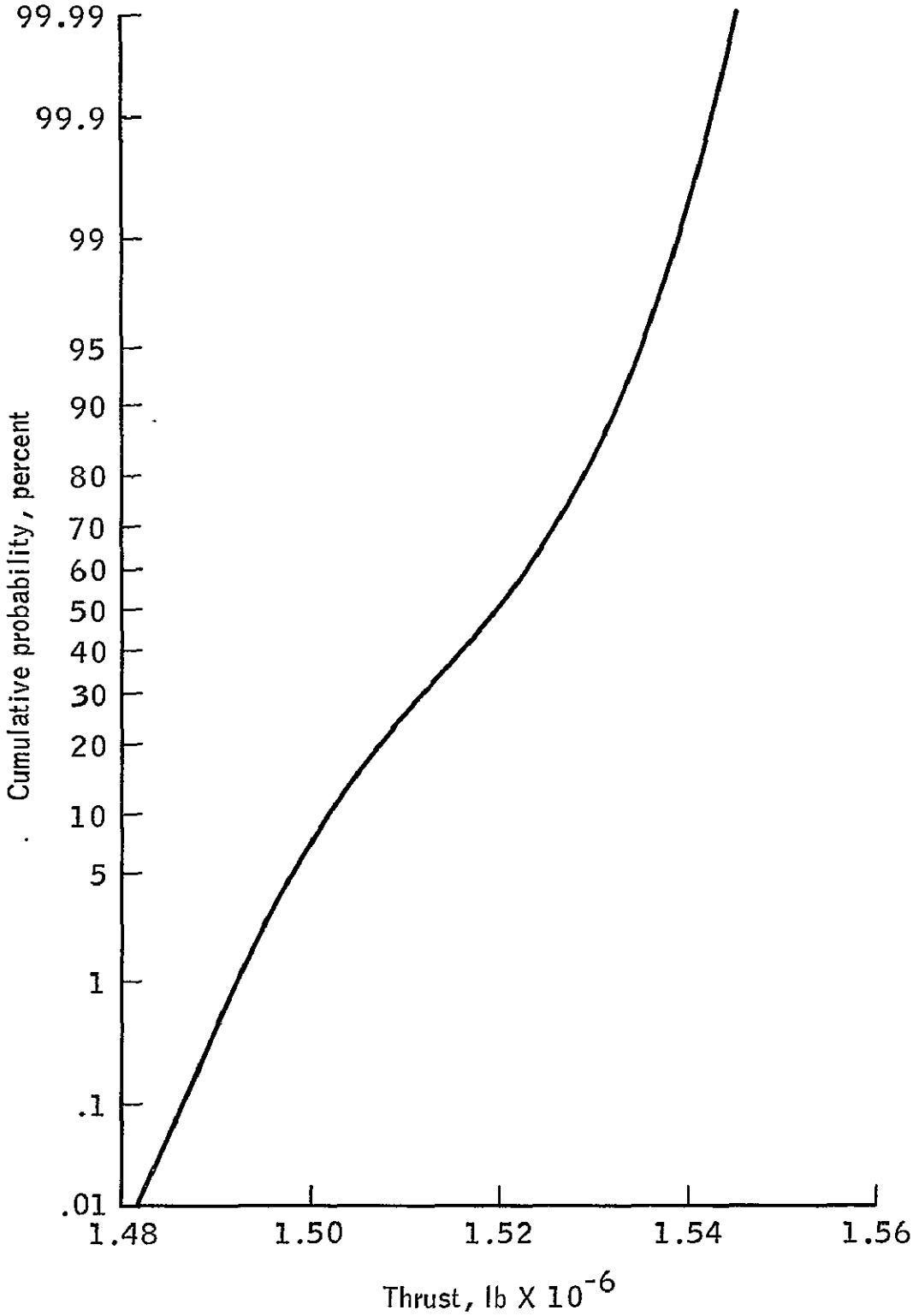

Figure 15.- Cumulative probability distribution of maximum thrust (per engine).

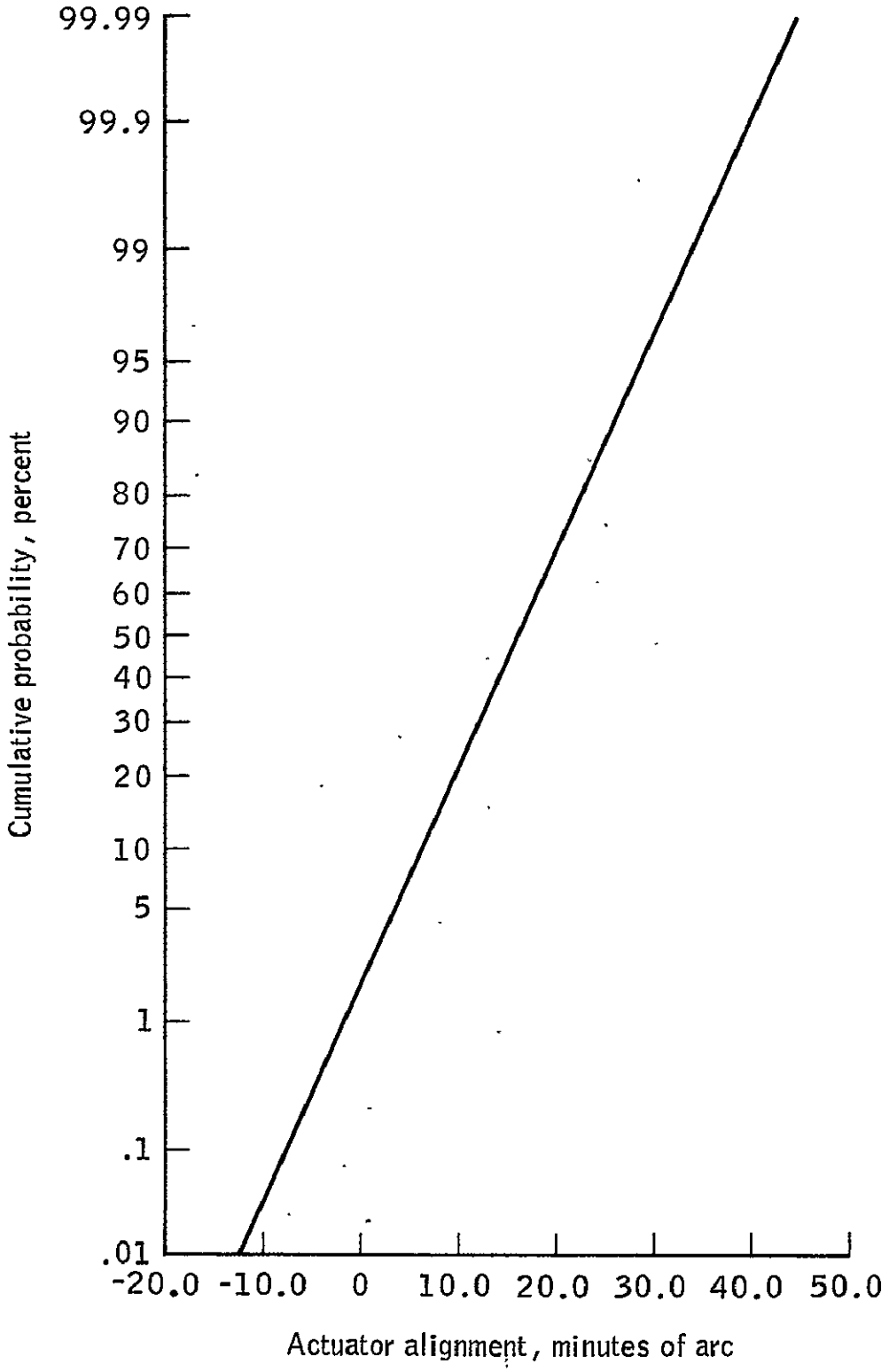

Figure 16.- Cumulative probability distribution of actuator 1 and 2 alignments.

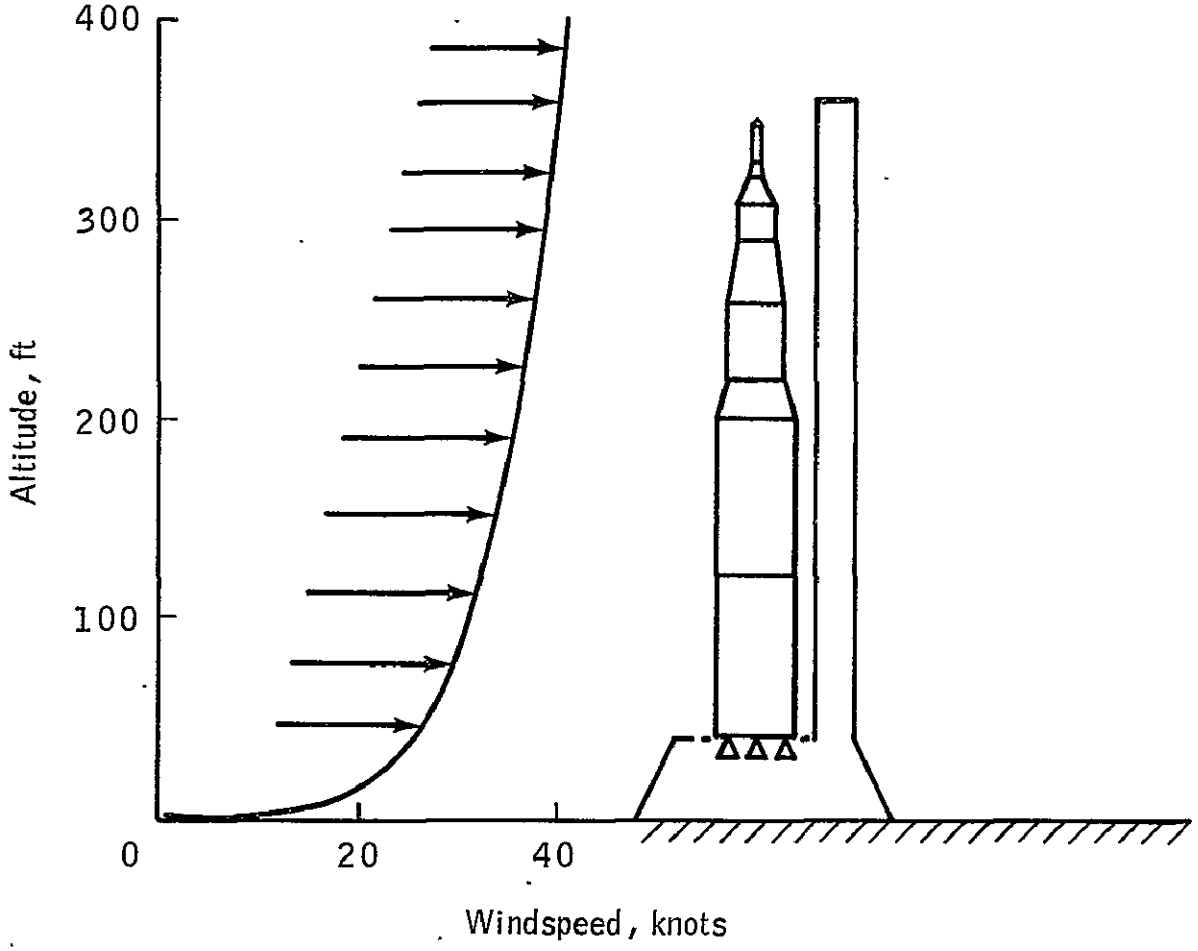

(a) Windspeed-altitude profile.

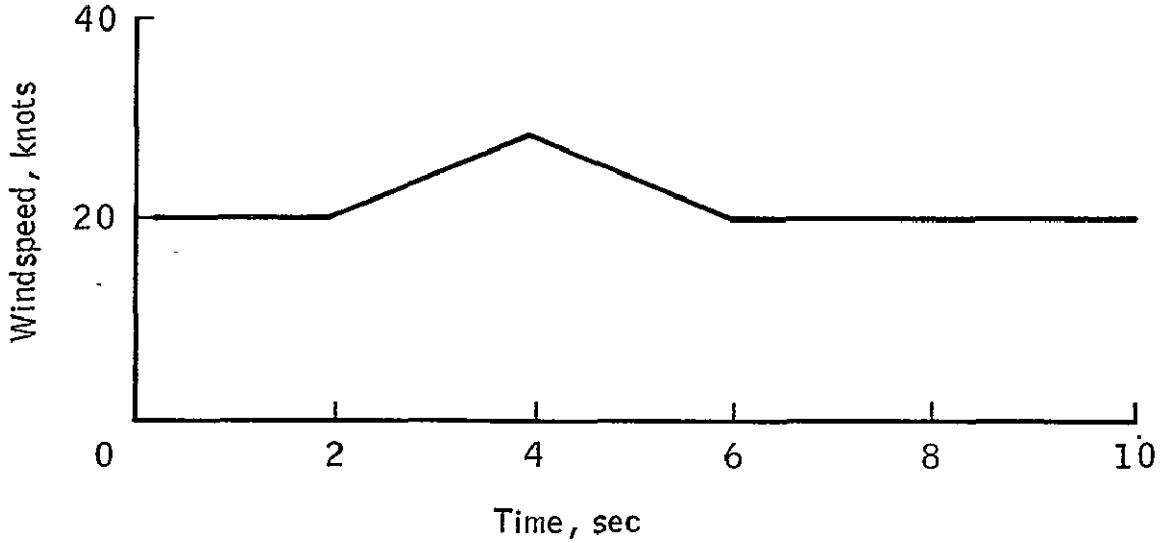

(b) Windspeed-time profile.

Figure 17.- Windspeed profiles.

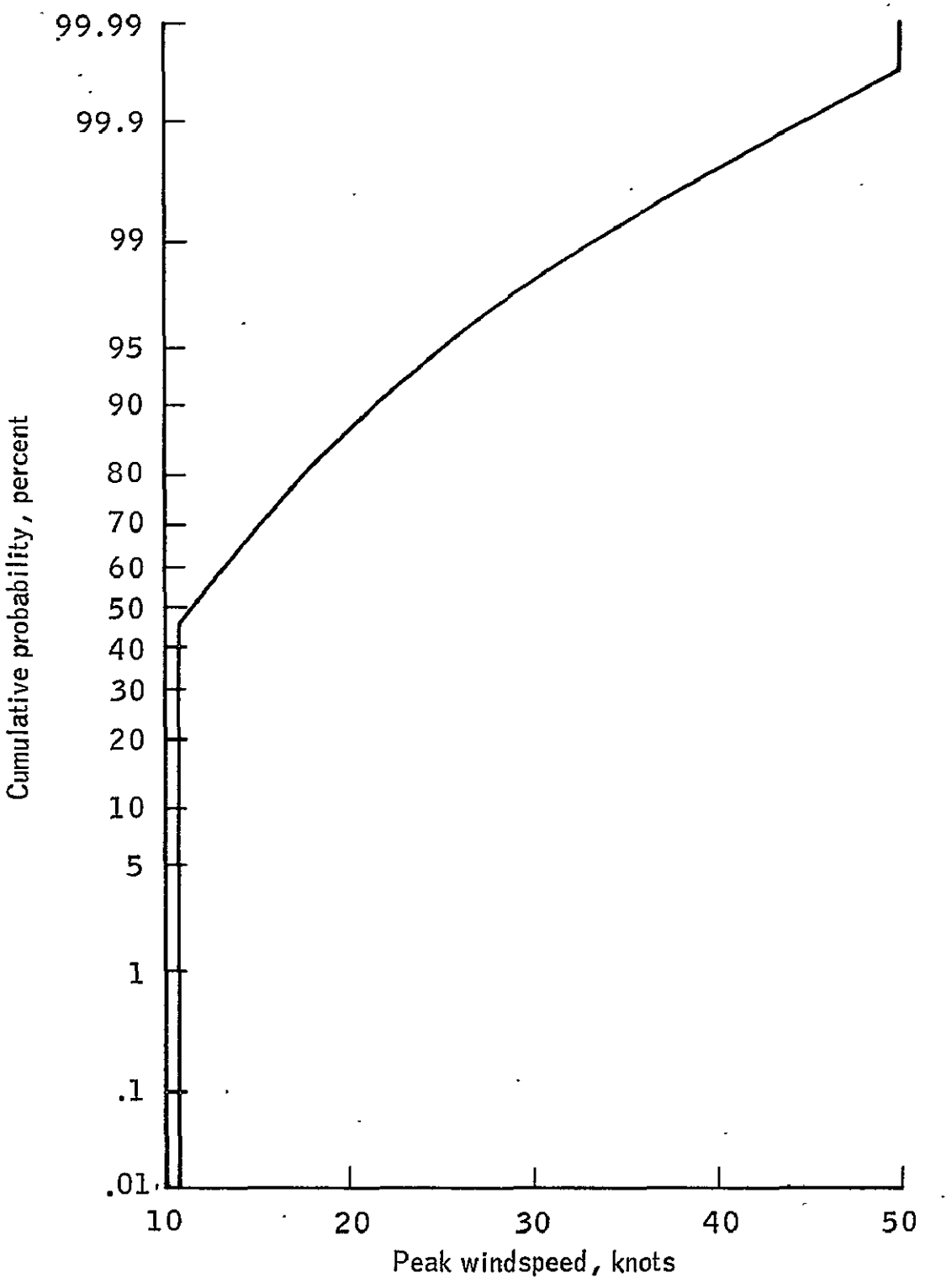

Figure 18.- Cumulative probability distribution of peak windspeed at 60 feet altitude.

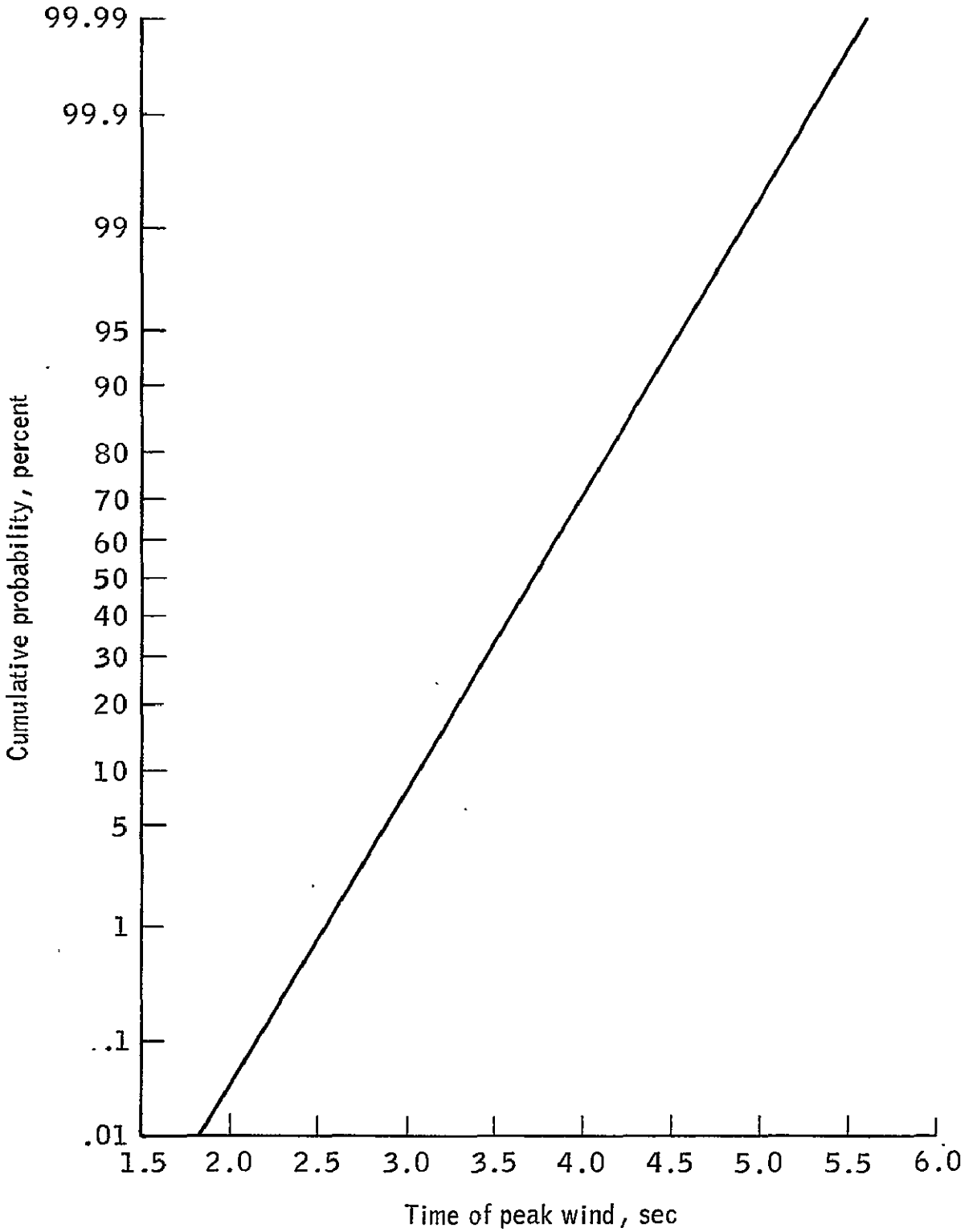

Figure 19.- Cumulative probability distribution of time at which windspeed peaks.

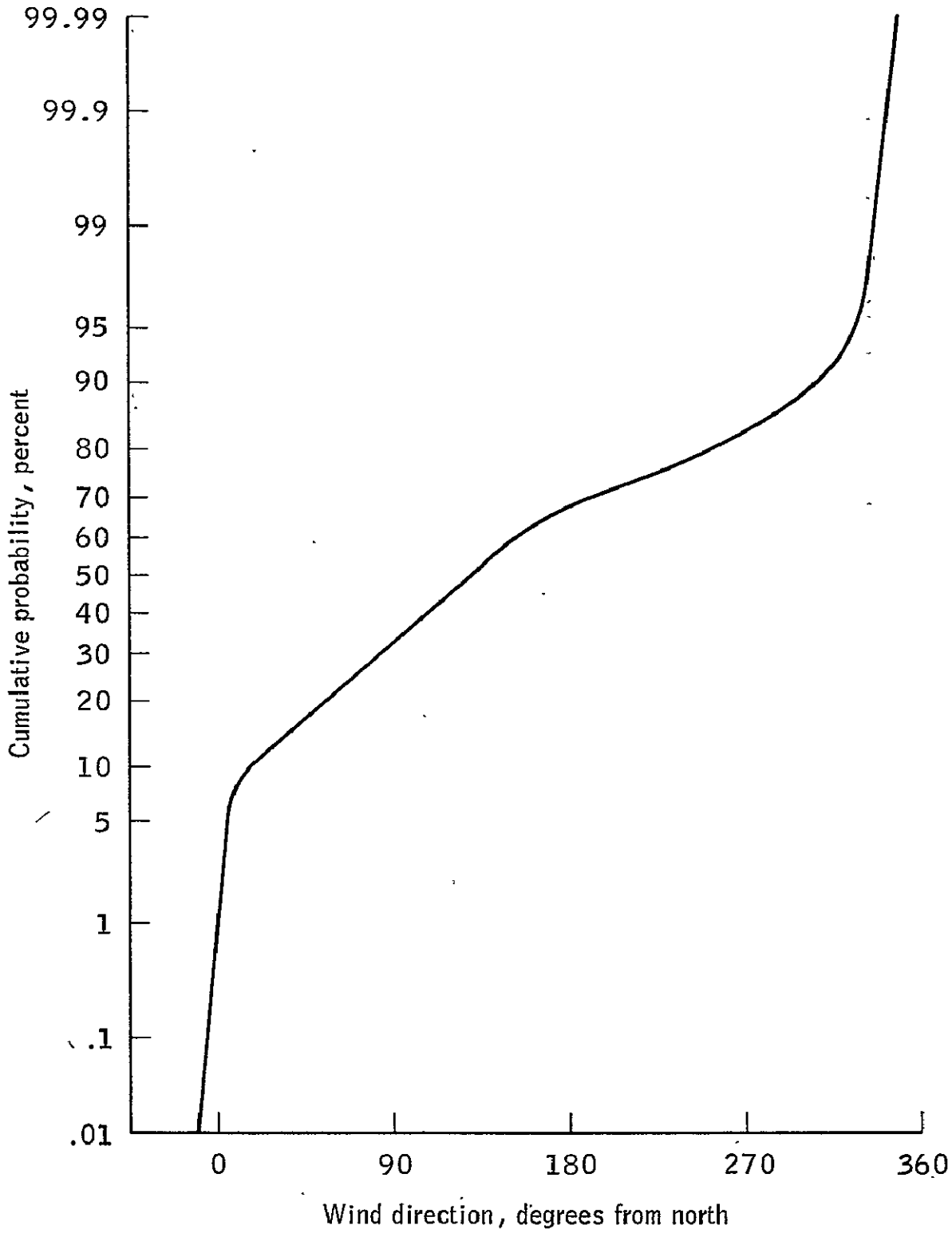

Figure 20.- Cumulative probability distribution of wind direction.

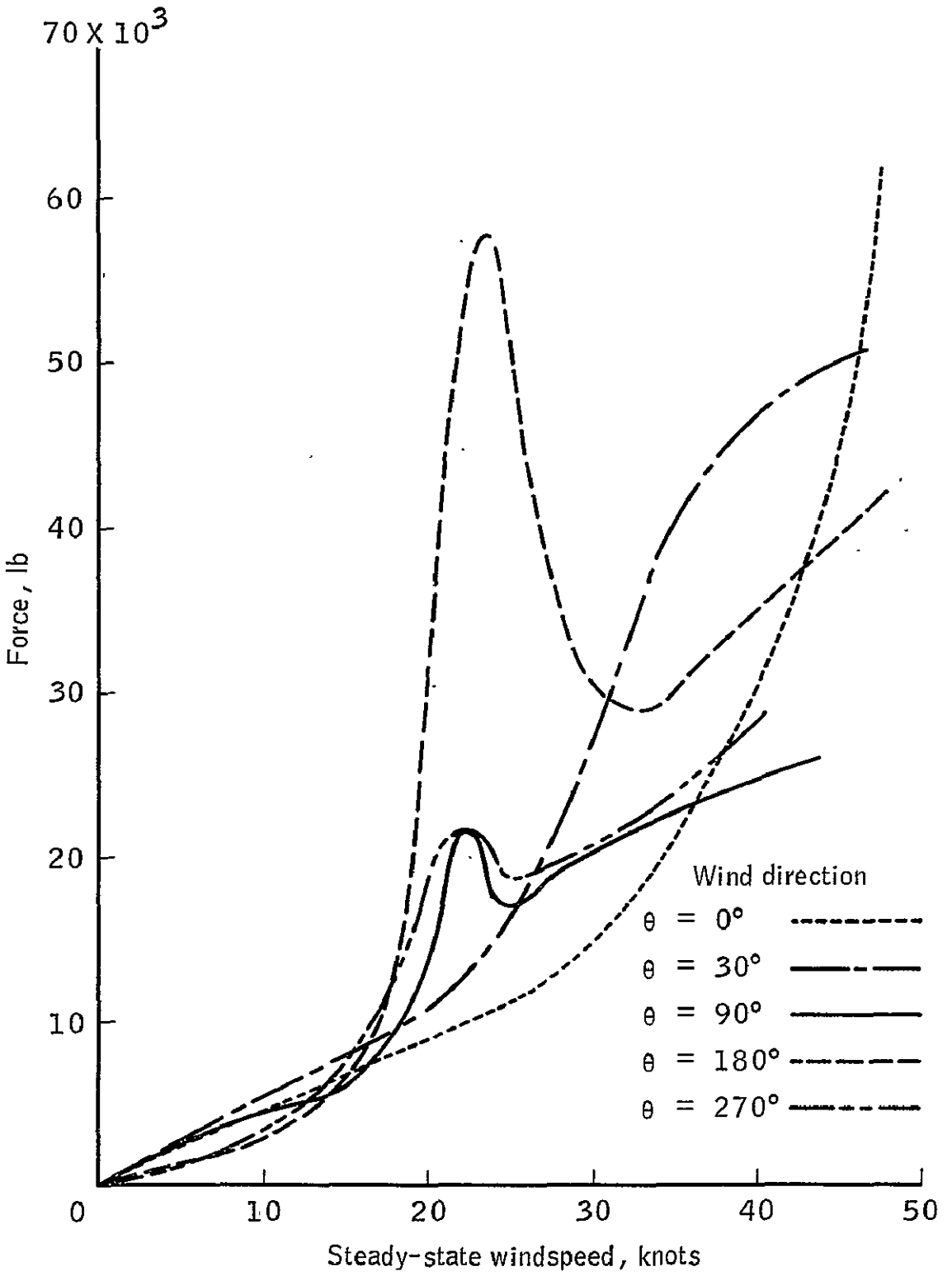

Figure 21.- Vortex shedding force versus windspeed and direction.

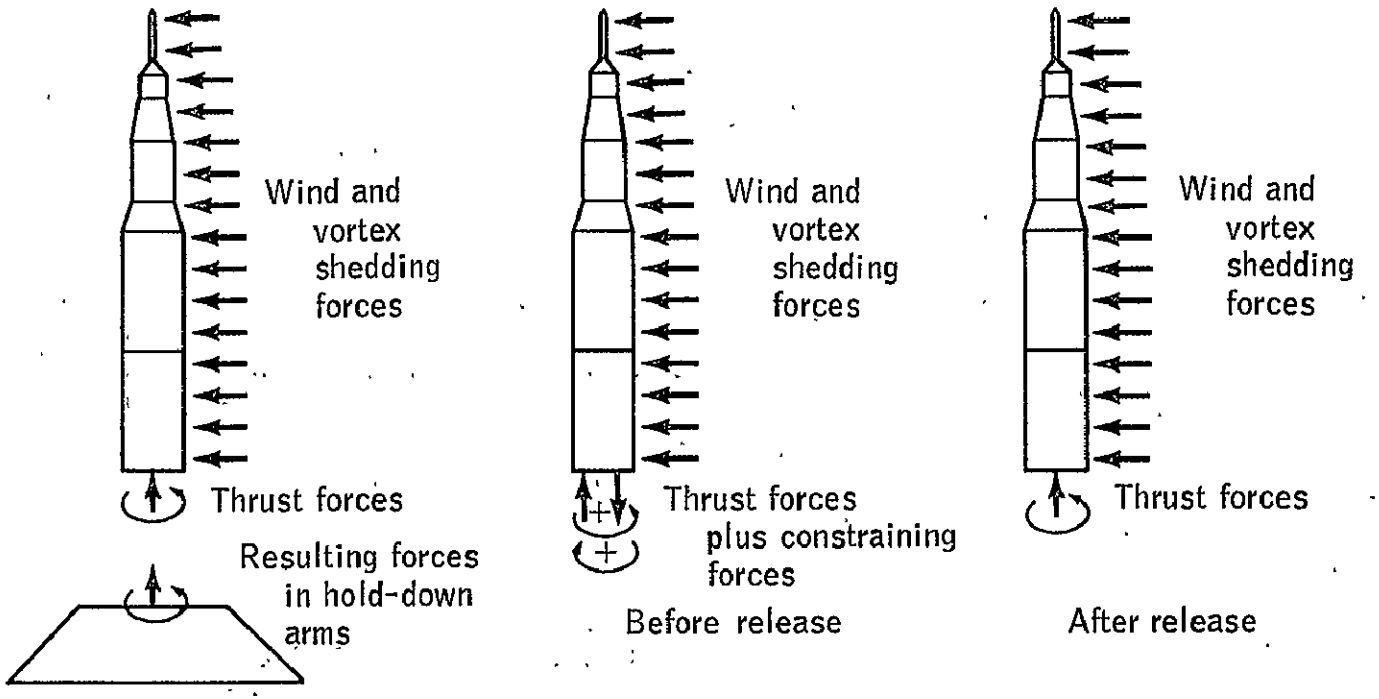

Figure 22.- Application of cantilever and free-free models to simulate launch release.

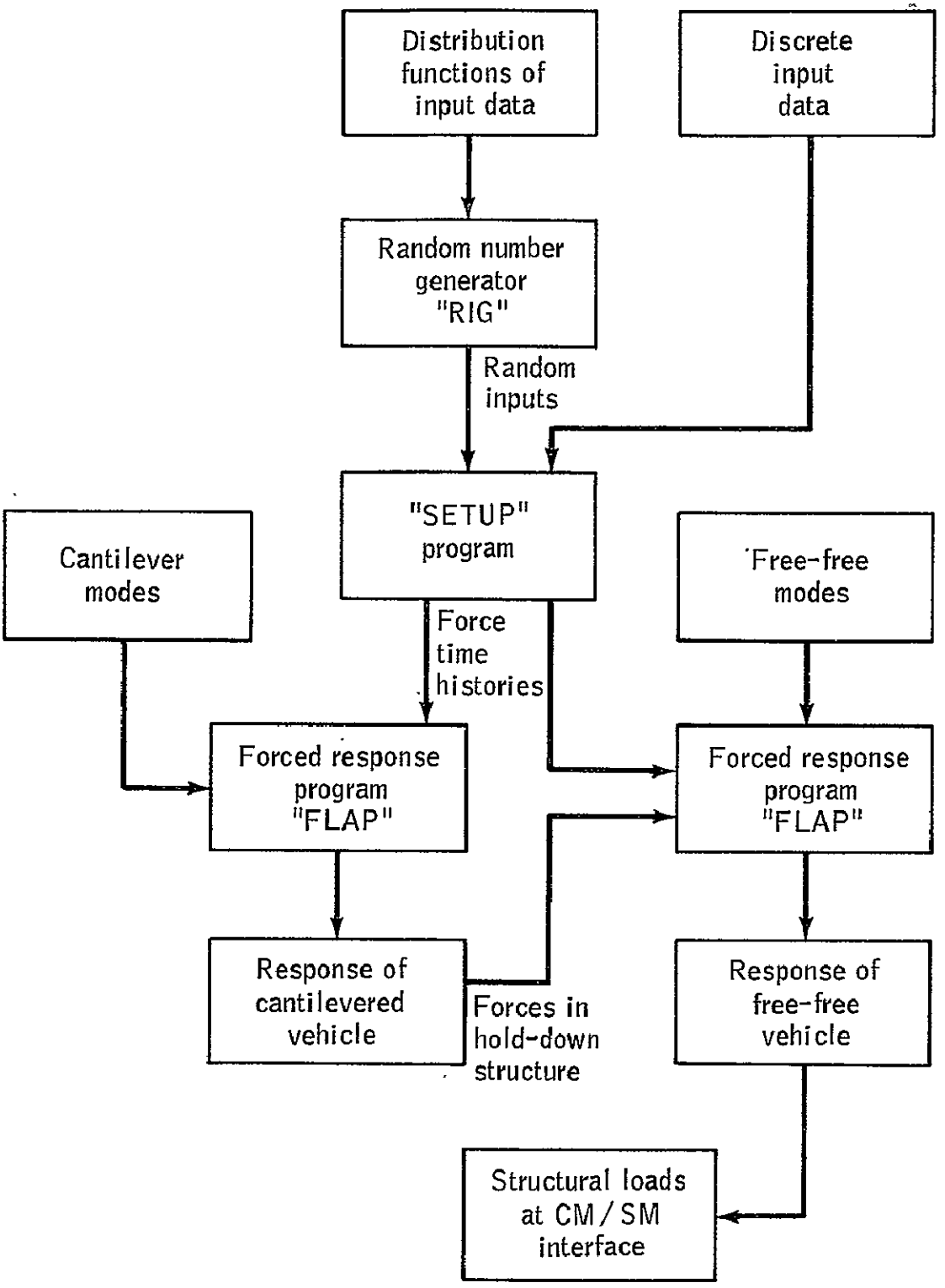

Figure 23.- Computer solution flow chart.

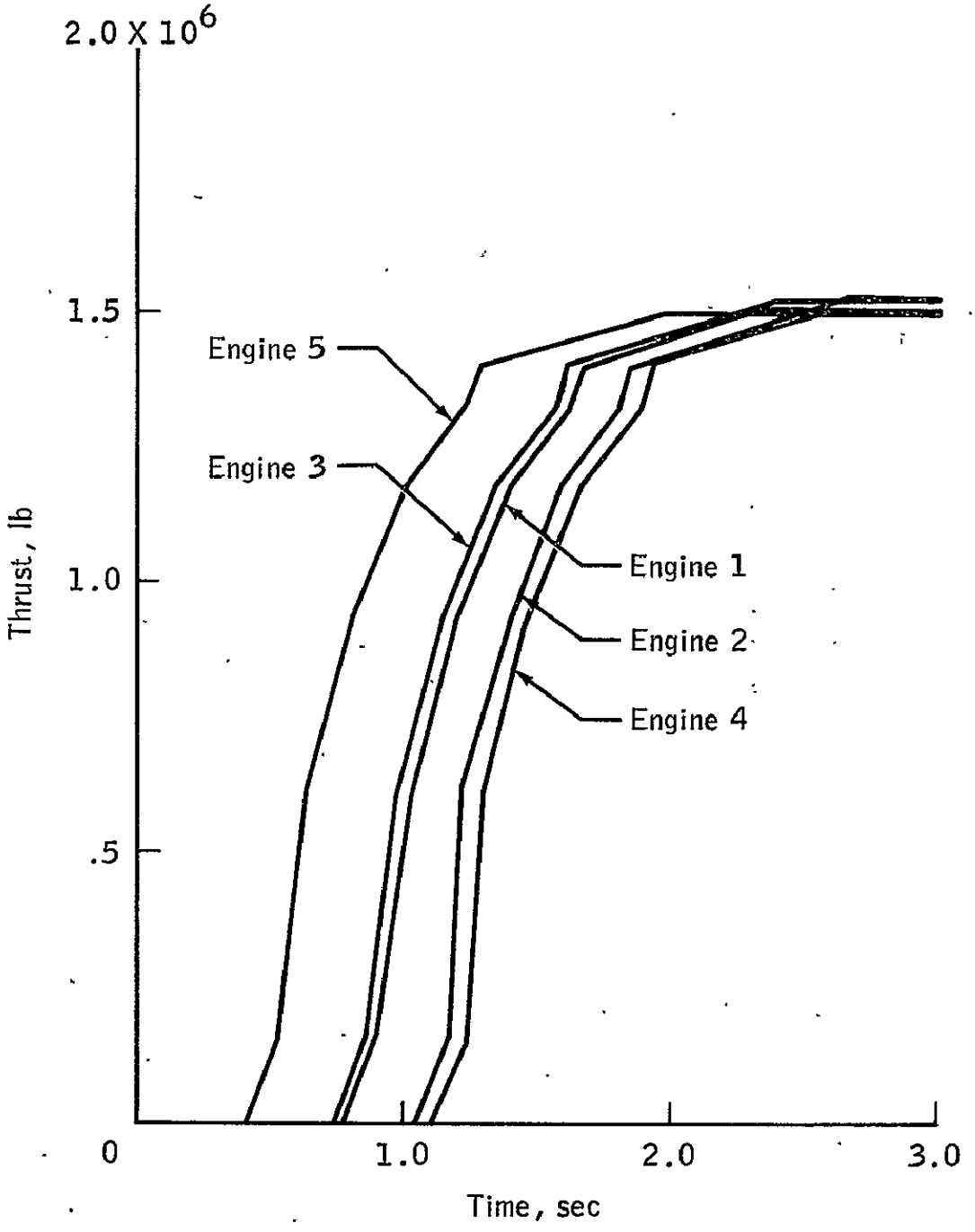

Figure 24.- Example thrust buildup curves.

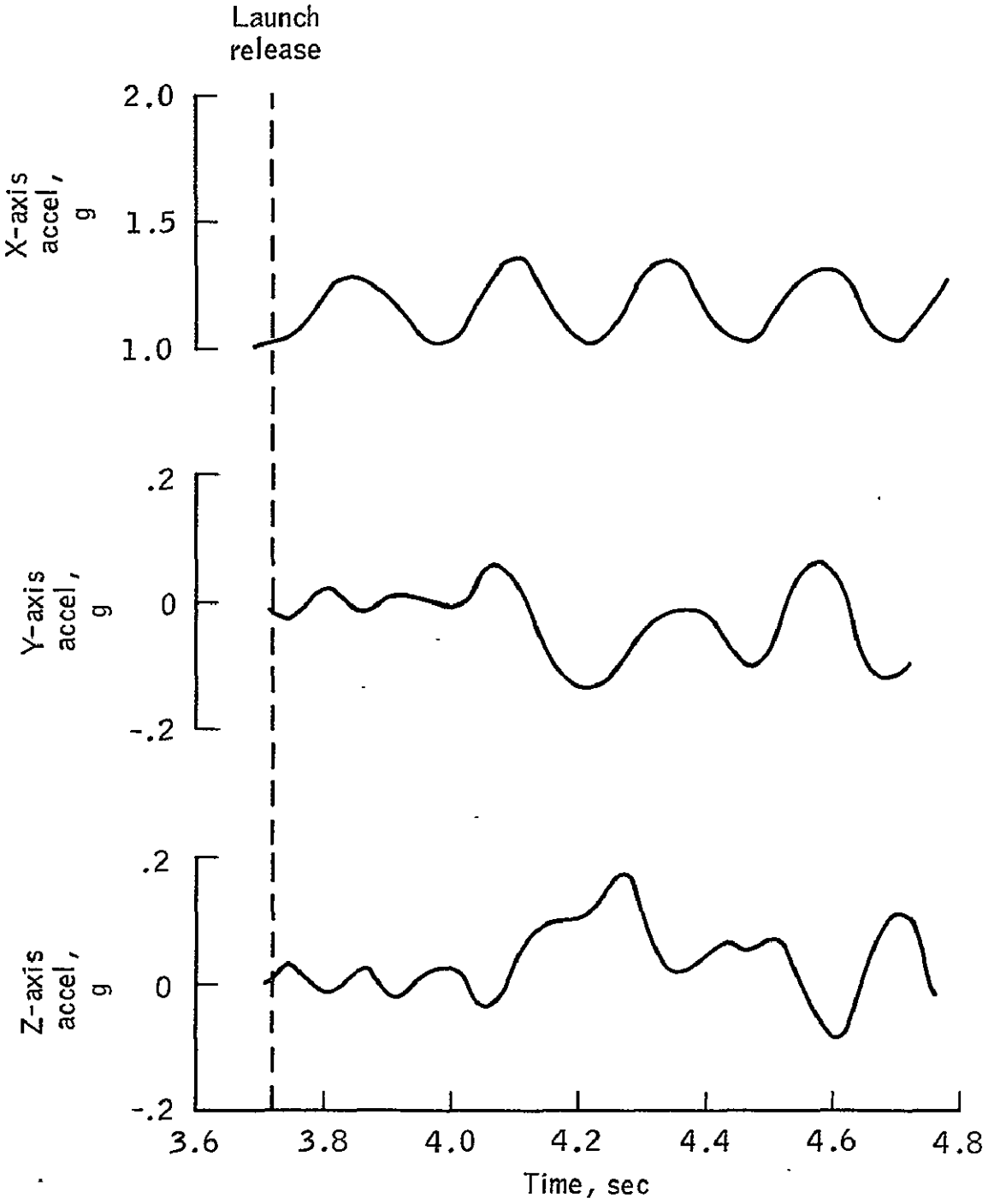

Figure 25.- Example of CM acceleration at launch release.

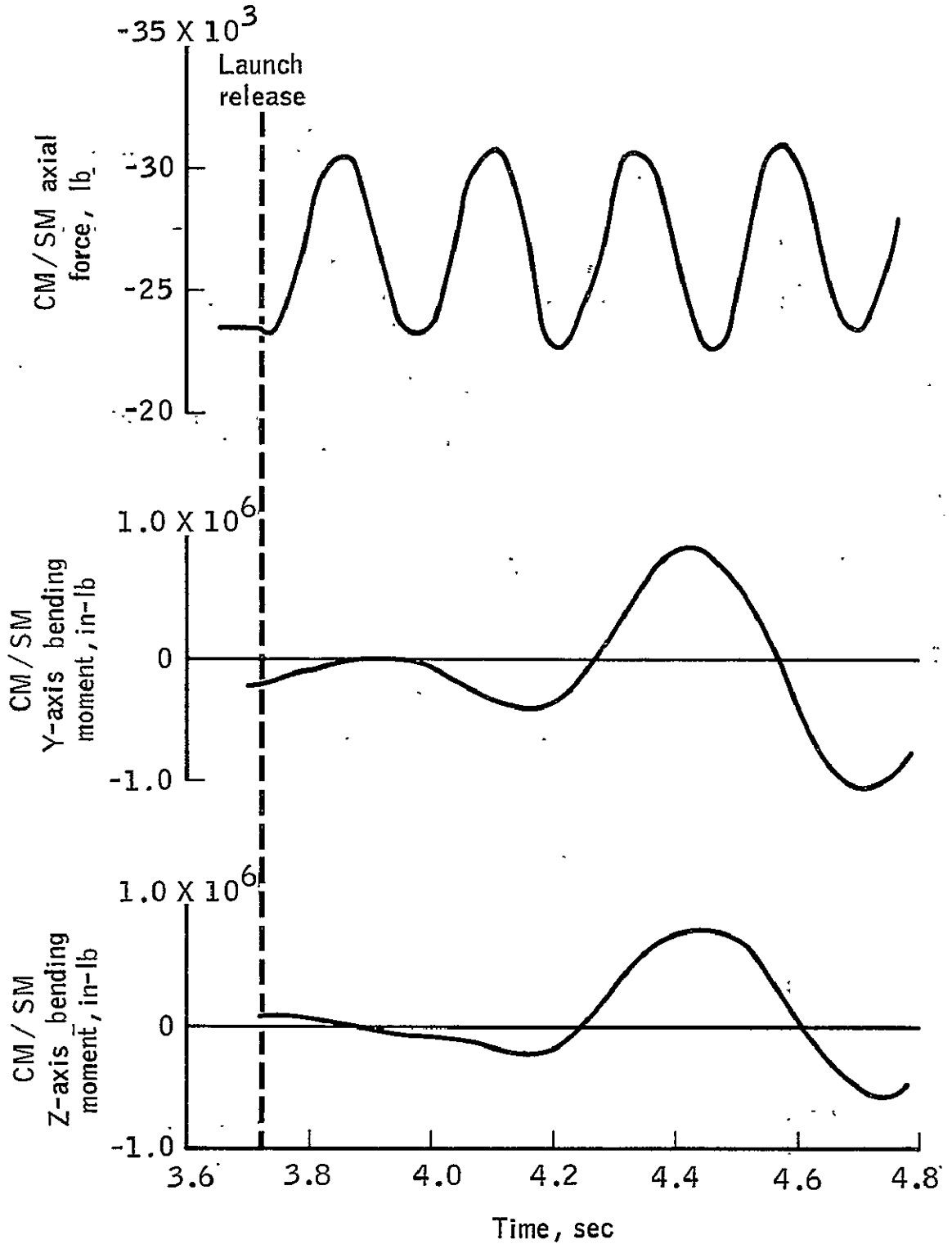

Figure 26.- Example of CM/SM interface axial and bending loads at launch release.

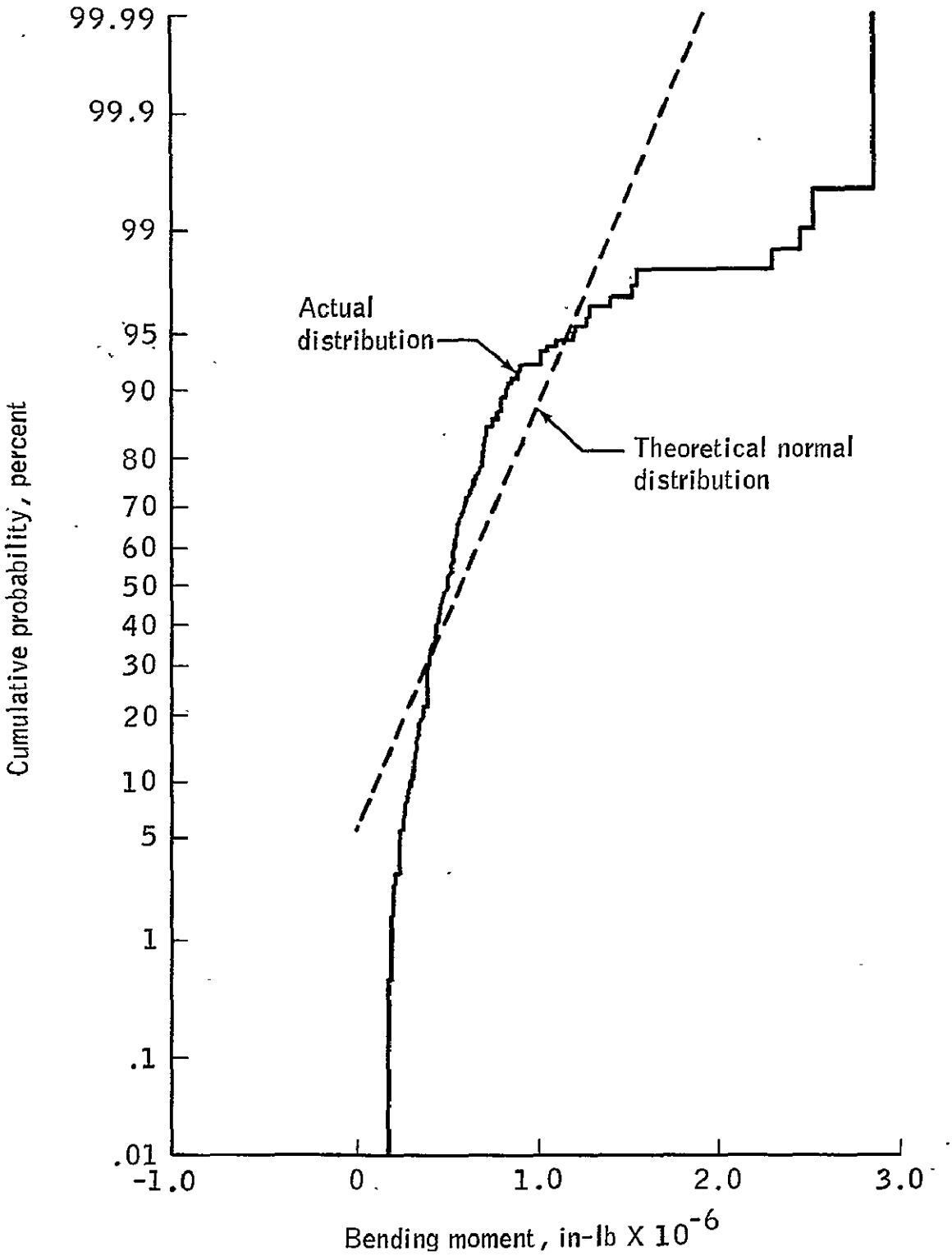

Figure 27.- Cumulative probability distribution of $M_{R_{max}}$.

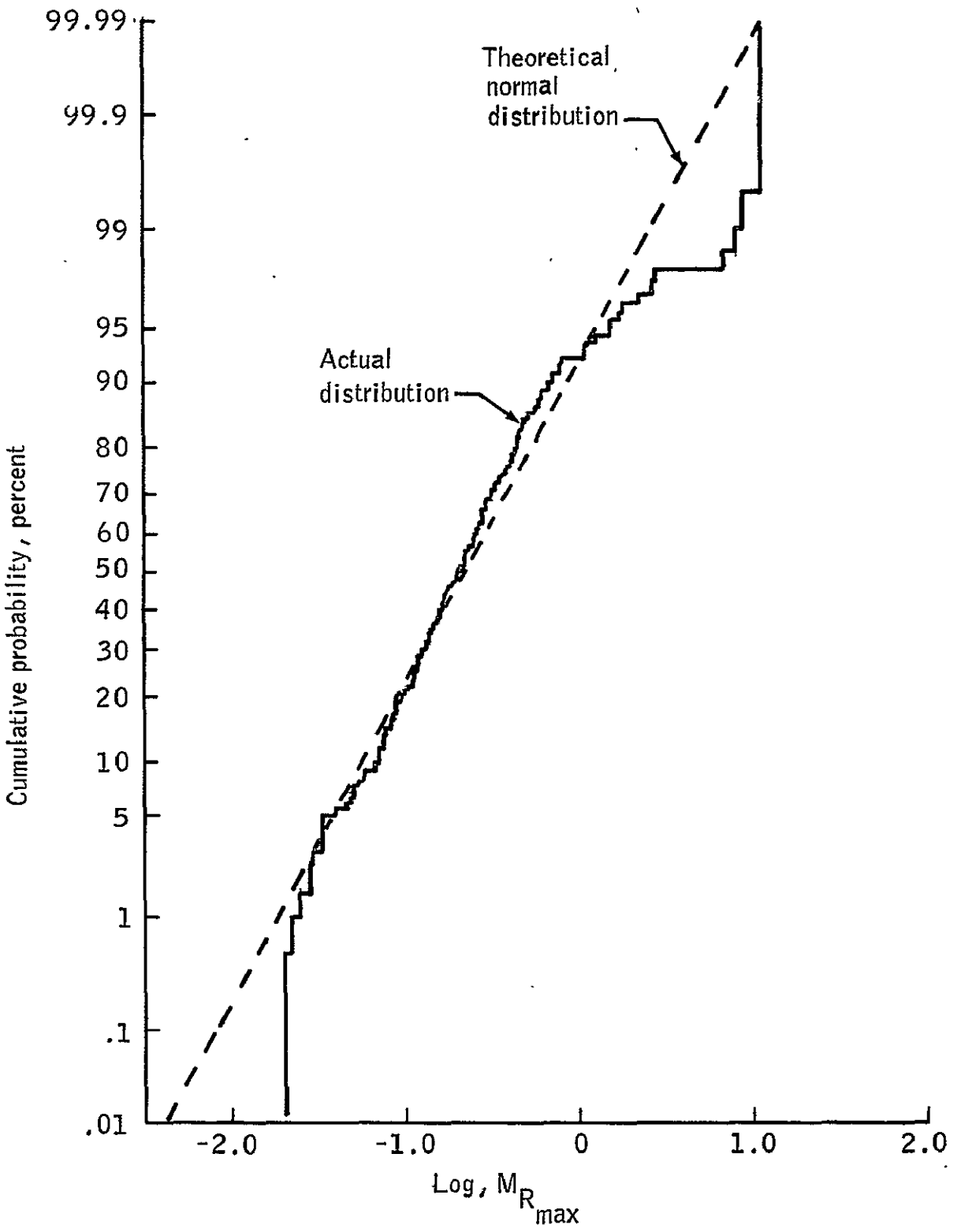

Figure 28.- Cumulative probability distribution of log $M_{R_{max}}$.

APPENDIXES

APPENDIX A

THE MONTE CARLO METHOD

A Monte Carlo method is generally described as one in which a given problem is simulated by some suitable random process. More specifically, it may be defined in application to this thesis as the statistical determination of a lift-off design load where the input data are first selected at random and the output data (structural loads) are then analyzed statistically. Random input data are selected and loads calculated for many cases in order to obtain a sample of output data adequate to define its distribution. In order to conduct and understand the results of such a study, a few principles of probability are necessary and are derived below.

Let the one-dimensional set A be such that

$$\int_A f(x)dx = 1 \qquad . \quad f(x) > 0$$

for all x in A and $f(x)$ has, at most, a finite number of discontinuities in every finite interval that is a subset of A.

If A is the sample space of the random variable X, and if the probability that X is in A is defined by $\int_A f(x)dx$, then X is a

continuous-type random variable with a probability density function (p.d.f.) $f(x)$. The cumulative distribution function F_x is now defined.

$$F_x = Pr[X \leq x] = \int_{-\infty}^{x} f(x)dx$$

Since $f(x) > 0$, F_x is a nondecreasing function.

Suppose now that x is one of the inputs to the problem and is described by its distribution function F_x. Assume also that to solve the problem it is desired to make n simulations requiring n random variables $X_1, \ldots, X_n$ from the distribution function F_x. To obtain a random sample of the variable X, it is sufficient to obtain a random sample of a variable Y, which is uniformly distributed over the interval 0 to 1. This follows from the fact that the distribution function F_x of the random variable X is a nondecreasing function ranging from 0 to 1. Consequently, $F_x^{-1}(y)$, an inverse function, may be defined for values of y between 0 and 1. $F_x^{-1}(y)$ is equal to the smallest value of x, satisfying the condition that $F_x \geq y$.

In terms of the inverse function $F_x^{-1}(y)$ to the distribution function F_x of the random variable X, the following theorem may be stated:

Let $Y_1, Y_2, \ldots, Y_m$ be independent random variables each uniformly distributed over the interval 0 to 1. The random variables defined by

$$X_1 = F_x^{-1}(Y_1) \qquad X_2 = F_x^{-1}(Y_2) \qquad \ldots \qquad X_n = F_x^{-1}(Y_n)$$

are then a random sample of the random variable X (Reference 5).

This theorem permits the selection of n random variables whose distribution function is known by selecting n random numbers uniformly distributed between 0 and 1.

The same principles apply also to the analysis of output data. The primary statistical quantity of interest in this Monte Carlo analysis is the probability that a given load will not be exceeded. For example, it may be desired that the design load be that which would not be exceeded 95 percent of the launches. With a finite sample size it is impossible to obtain the exact 95-percent load, but a point estimate of this quantity is possible. This point estimate is obtained in the following manner. If the load can be assumed to be normally distributed with mean μ and variance σ^2 then the true 95-percent load is

$$F_{.95} = \mu + K_{.95}\sigma$$

The corresponding point estimate of this load is given by

$$F'_{.95} = \overline{F} + K_{.95} \cdot S$$

where

$$\overline{F} = \frac{1}{N} \sum_{i=1}^{N} F_i$$

and

$$S^2 = \frac{1}{N - 1} \sum_{i=1}^{N} \left(F_i - \overline{F} \right)^2$$

where $\overline{F}$ is the sample mean and S^2 is the sample variance. The square root of the sample variance S is called the standard deviation and N is the number of cases in the sample. The value of the constant $K_{.95}$ is 1.645 as obtained from a table of normal percentage points. The above are unbiased estimates of the mean and standard deviation of the entire population. The sample, variance, however, if calculated from

$$S^2 = \frac{1}{N} \sum_{i=1}^{N} \left(F_i - \overline{F}\right)^2$$

would not be an unbiased estimate of the variance of the population. The sum of the squares of deviation of the individual sample values from the sample mean results in the minimum sum of squares of deviation. The sum of squares of deviation from any value other than the mean will be larger than from the mean. Since the sample mean may not be identical with the population mean, the sum of squares of deviation of the individual sample values from the sample mean would be less than the sum of the squares of deviation of the individual sample values from the population mean. The standard deviation of the sample, computed from the sum of the squares of deviation divided by N would therefore be smaller than if the sum of squares had been calculated from the true population mean. To overcome this bias, the variance estimated from the sample is obtained by dividing the sum of squares of deviation by $N - 1$ instead of by N (Reference 6).

The statistical estimates described above are based on the assumption that the underlying loads distribution is normal. The validity of this assumption can be investigated by means of the χ^2 goodness of fit test. The N loads should first be ordered from minimum to maximum

values and a cumulative distribution function plotted. Then the N loads are classified to m mutually exclusive intervals. The number of observations in each interval is n_i, i = 1, 2, ..., m. Then the number of expected observations (e_i, i = 1, 2, ..., m), which according to the theoretical distribution should fall into each interval, are calculated. The following statistic is then calculated.

$$\chi^2_{m-3} = \sum_{i=1}^{m} \frac{(n_i - e_1)^2}{e_i}$$

If the observed and theoretical probability distributions are identical, the χ^2 test statistic is distributed according to the χ^2 probability law with m - three degrees of freedom. The degrees of freedom which enter into the evaluation of χ^2 are the number of independent observations that are available for its calculation (Reference 4). Thus m intervals provide m - 1 independent intervals. The expected observations depend on the two-point estimates of the mean and variance. Thus, the number of independent observations are m - 1 - 2 = m - 3.

If the observed and theoretical probability distributions are identical, the value of the χ^2 test statistic will be small. The probability of occurrence of any given value of the test statistic may be determined from a table of χ^2 percentage points. For example, if the calculated value of the test statistic for 12 degrees of freedom is 18.5, then the corresponding probability is 10 percent that the variation of the observed loads from the theoretical distribution would exceed

the calculated variation, even if the observed and theoretical distributions were identical. For individual data quantities in engineering practice, the hypothesis of identical distributions is usually rejected at the 5-percent level.

APPENDIX B

PROGRAM "SETUP"

The "SETUP" program is the only computer program developed specifically for this thesis. Its sole purpose is to accept the randomly generated data from "RIG" in card format and setup forcing functions acceptable to the "FLAP" program. Symbols used in this program are listed at the end of this appendix.

Forces Required

"SETUP" is used for this study to setup forcing functions for the program "FLAP" for each case. To do this it must accept randomly generated data from "RIG" and establish discrete force versus time tables. Outputs include F_{T_1}, F_{T_2}, and F_{T_3} which are the x, y, and z, components of thrust acting on the corresponding degrees of freedom of the thrust structure. F_{T_4} and F_{T_5} are thrust-induced turning moments applied to the y and z rotational degrees of freedom at the same node. F_{T_6} and F_{T_7} are the y and z components of the vortex shedding force applied as a constant to the node closest to the launch vehicle center of pressure. F_{T_8} and F_{T_9} through $F_{T_{38}}$ and $F_{T_{39}}$ are alternately the y and z components of drag force time histories applied to 16 nodes along the vehicle.

Equations

a. Wind profile, W_i versus t_{W_i}

$W_1 = V_{peak}/1.4$ $\quad t_{W_1} = 0.0$

$W_2 = W_1$ $\quad t_{W_2} = t_{peak} - 2.0$

$W_3 = V_{peak}$ $\quad t_{W_3} = t_{peak}$

$W_4 = W_1$ $\quad t_{W_4} = t_{peak} + 2.0$

$W_5 = W_1$ $\quad t_{W_5} = 10.0$

b. Thrust curves, T_{ij} versus t_{ij}

$T_{i1} = F_1$ $\quad t_{i1} = 0.0$

$T_{i2} = F_2$ $\quad t_{i2} = t_i + \Delta t_i$

$T_{i3} = F_3$ $\quad t_{i3} = t_{i2} + 0.12$

$T_{i4} = F_4$ $\quad t_{i4} = t_{i3} + \left(0.534 \times 10^6/R_{1i}\right)$

$T_{i5} = F_5$ $\quad t_{i5} = t_{i4} + 0.164$

$T_{i6} = F_6$ $\quad t_{i6} = t_{i5} + 0.2$

$T_{i7} = F_7$ $\quad t_{i7} = t_{i6} + 0.22$

$T_{i8} = F_8$ $\quad t_{i8} = t_{i7} + \left(0.08 \times 10^6/R_{2i}\right)$

$T_{i9} = F_{max_i}$ $\quad t_{i9} = t_{i2} + 1.55$

$T_{i10} = F_{max_i}$ $\quad t_{i10} = 10.0$

Because the "FLAP" program requires identical time tables for all forces, the above wind profile and thrust curves are interpolated at 50 time points. The following force outputs are calculated for each of those time points.

c. Force outputs

The following equations are used to calculate the thrust forces at the jth time point.

$$F_{T_1} = \sum_{i=1}^{5} T_{ij}$$

$$F_{T_2} = (-\cos 45°)\Big[T_{ij}(\beta_{12} - \beta_{11}) - T_{2j}(\beta_{21} + \beta_{22}) + T_{3j}(\beta_{31} - \beta_{32}) + T_{4j}(\beta_{41} + \beta_{42}) + T_{5j}(\beta_{52} - \beta_{51})\Big]$$

$$F_{T_3} = (-\cos 45°)\Big[T_{ij}(\beta_{11} + \beta_{12}) + T_{2j}(\beta_{22} - \beta_{21}) - T_{3j}(\beta_{31} + \beta_{32}) + T_{4j}(\beta_{41} - \beta_{42}) + T_{5j}(\beta_{51} + \beta_{52})\Big]$$

$$F_{T_4} = 128.7(T_{ij} + T_{4j} - T_{2j} - T_{3j})$$

$$F_{T_5} = 128.7(T_{ij} + T_{2j} - T_{3j} - T_{4j})$$

The following equations are used to calculate the constant components of vortex shedding force.

$$F_{T_6} = (F_{vort})(\sin \theta_w)$$

$$F_{T_7} = (F_{vort})(\cos \theta_w)$$

The remaining equations in the program are used to calculate the y and z components of aerodynamic drag at each of 16 vehicle nodes at the jth time point

$$F_{w_{ij}} = A_i\left(W_j\right)^2 \qquad i = 1 \text{ to } 16$$

$$F_{T_8} = \left(-\cos\theta_w\right)F_{w_j}$$

$$F_{T_9} = \left(\sin\theta_w\right)F_{w_j}$$

$$F_{T_{10}} = \left(-\cos\theta_w\right)F_{w_{2j}}$$

$$F_{T_{11}} = \left(\sin\theta_w\right)F_{w_{2j}}$$

.

.

.

$$F_{T_{38}} = \left(-\cos\theta_w\right)F_{w_{16j}}$$

$$F_{T_{39}} = \left(\sin\theta_w\right)F_{w_{16j}}$$

"SETUP" Symbols

A_i coefficient to determine ith drag force from windspeed at reference height, lb/knot^2

F_j nominal thrust at jth time point, lb

F_{max_i} maximum thrust of ith engine, selected from Figure 15

F_{T_i} ith force time history applied to a vehicle node, lb

$F_{w_{ij}}$ total drag force at ith node and jth time point, lb

R_{1i} initial buildup rate of ith engine thrust, selected from Figure 13, lb/sec

R_{2i} second buildup rate of ith engine thrust, selected from Figure 14, lb/sec

t_i nominal ignition time of ith engine, sec

T_{ij} thrust of ith engine at jth time point, lb

t_{ij} adjusted jth time point for ith engine thrust, sec

t_{peak} time point at which wind speed will peak, selected from Figure 19, sec

t_{w_i} time point associated with ith wind speed, sec

V_{peak} peak wind speed at the 60-foot reference height selected from Figure 18, knots

W_i wind speed at the 60-foot reference height at ith time point, knots

β_{ij} misalignment of ith engine in actuator position j, selected from Figure 16, radians

Δt_i variation in ith engine ignition time selected from Figure 10, sec

θ_w direction from which wind is blowing, selected from Figure 20, deg

Intervals	Probability	Observed frequency	Expected frequency	$\frac{(n_i - e_i)^2}{e_i}$
7	0.0667	10	13.333	0.833
8	.0667	16	13.333	.535
9	.0667	18	13.333	1.634
10	.0667	15	13.333	.208
11	.0667	12	13.333	.133
12	.0667	13	13.333	.008
13	.0667	10	13.333	.833
14	.0667	6	13.333	4.033
15	.0667	13	13.333	.008
Total	1.00	200	200.00	$\chi^2 = 17.35$

The value of the χ^2 test statistic is therefore 17.35. Having chosen 15 intervals, the validity of the lognormal distribution assumption must be determined from the χ^2 table of probability levels for $15 - 3 = 12$ degrees of freedom. From the table, the probability of finding a χ^2 statistic greater than 17.35 for 12 degrees of freedom is approximately 16 percent. This means that even if the hypothesis of $M_{R_{max}}$ being lognormally distributed were correct, the probability of finding a χ^2 statistic larger than 17.35 is 16 percent. Since the 5-percent level test was easily satisfied, the hypothesis is accepted.

APPENDIX C

THE χ^2 TEST OF LOAD DISTRIBUTION

The χ^2 goodness of fit test described in Appendix A was applied to the observed and theoretical distributions of $\log (M_{R_{max}})$ shown in Figure 28. Fifteen discrete intervals of equal probability were used to calculate the following χ^2 statistic.

$$\chi^2 = \sum_{i=1}^{15} \frac{(n_i - e_i)^2}{e_i}$$

where n_i is the observed frequency (observed number of points to fall within the ith interval) and e_i is the expected frequency (expected number to fall within the ith interval, i.e., $\frac{200}{15}$).

The following table shows the calculation of the χ^2 statistic. The observed frequency was taken from the distribution function of Figure 28.

Intervals	Probability	Observed frequency	Expected frequency	$\frac{(n_i - e_i)^2}{e_i}$
1	0.0667	11	13.333	0.408
2	.0667	9	13.333	1.408
3	.0667	14	13.333	.033
4	.0667	13	13.333	.008
5	.0667	22	13.333	5.634
6	.0667	18	13.333	1.634

1 STOCK LOCATION

2 DATE RECEIVED YR 70 MO 7 DAY 22

12 SCREEN ☐ REJECT ☐ OBTAIN BETTER COPY ☐ OUT OF PRINT SOD ☐ OBTAIN AUTHORITY ☐ ERRATA

17 ACCESSION NUMBER N70-30385

3 RECEIPT TYPE & FORMAT ☐ MAGNETIC TAPE ☐ LOAN ☒ PC ☐ 35 MM ☐ CARDS ☒ RETAIN ☐ MF ☐ 16 MM ☐ OTHER →

13A ANNOUNCEMENT VOL ISSUE ☒ USG ☐ TAB ☐ UNANN

13B FAS ☐ YES ☒ NO R

18 PAGES 92

19 SHEETS —

20 LOW LIMIT PC MF

21 ☐ SUB-SCRIP-TION

4 STOCK RECEIVED FOR SALE PC 20 MF

14 REPRODUCTION INSTRUCTIONS

BB→ PRINT ↓	NO	1UP	2UP
NO	1	4	7
1UP	2	5	8
2UP	3	6	9
MIX	SAME SIZE	ORDER STOCK FROM	0

MAKE MICROFICHE ☐ YES ☒ NO ☐ ON DEMAND

22 PRICES PC ☒ MF ☒ 3.00 0.65

EXCEPTION PRICES

23 CATEGORY

5 LOAN DOCUMENT RETURNED

DUE

OUT

24 DISTR CODE —

25 INITIALS ACC VH A B C D

6 TRANSACTION NEW ITEM ☒ DUPE ☐ SUPER-SEDES ☐ PRIOR NUMBER ☐

15 PRESTOCK

	NOI	# COPIES
PC	X	
MF		M
PC DUE IN		

26 FILL FROM PAPER COPY ETC SS ☐ MICRO-NEGA-TIVE XN

27 PUBLIC RELEAS-ABILITY C

7

8 SERIES NUMBERS (X-REF) ☐→ NASA-TMX-58046

16 REMARKS NASA

9 RELATED DOCUMENT ☐→

9/3

1 ARCHIVES

0 CONTRACTING OFFICE NASA

11 NOT FULLY LEGIBLE ☐ COLOR ☐

FORM NBS 801 (7/69)

* GPO 1968—315-288

U.S. DEPARTMENT OF COMMERCE
NATIONAL BUREAU OF STANDARDS
CLEARINGHOUSE FOR FEDERAL SCIENTIFIC AND TECHNICAL INFORMATION

DOCUMENT TRAVELER